

Early-type stars as tracers of stellar (binary) evolution and violent ejection events

Habilitationsschrift
der Naturwissenschaftlichen Fakultät
der Friedrich-Alexander-Universität Erlangen-Nürnberg

vorgelegt von
Andreas Irrgang
aus Cham

Fachmentorat:

Prof. Dr. Ulrich Heber (Vorsitzender)

Prof. Dr. Uli Katz

Prof. Dr. Stefan Dreizler (Universität Göttingen)

Contents

Abstract	4
1 Introduction	5
2 Modeling of atmospheres and spectrophotometric analyses	7
2.1 Enhancements of the spectral fitting method	7
2.2 Improvements in the computation of synthetic spectra	7
2.3 A simple but powerful tool to study spectral energy distributions	8
2.4 Exemplary applications	10
2.4.1 Investigation of the ^3He anomaly	11
2.4.2 High-precision quantitative abundance studies	11
2.4.3 Computation of a grid of spectra for subdwarf B- and O-type stars	12
3 Constraining stellar models via pulsating and/or stripped stars	12
3.1 A pulsating B star as testbed for main sequence stellar evolution	22
3.2 A proto-helium white dwarf stripped via common-envelope ejection	24
3.3 A stripped B-type star in the potential black hole binary LB-1	24
3.4 A recently stripped, pulsating core of a massive star	26
4 Origin of hypervelocity and runaway stars	26
4.1 Hypervelocity stars (HVSs)	28
4.2 Runaway stars	28
4.2.1 Binary supernova scenario	28
4.2.2 Dynamical ejection scenario	29
4.2.3 Dynamical ejection and subsequent supernova disruption	30
4.3 High-velocity early-type stars in the <i>Gaia</i> era based on DR2	30
4.3.1 Revisiting the most promising HVS candidates from the HVS survey	30
4.3.2 An extreme runaway B star challenging classical ejection mechanisms	30
4.3.3 Revisiting (almost) all HVS candidates from the HVS survey	31
4.3.4 Searching for new runaway blue MS stars at high Galactic latitudes	31
4.4 High-velocity stars in the <i>Gaia</i> era based on EDR3	32
4.5 The need for an alternative ejection mechanism	32
Bibliography	36
Acknowledgements	37
Appended papers	38

Abstract

The goal of this habilitation thesis is to advance our understanding of stellar structure and evolution theory by providing guidance by observation. To this end, individual early-type stars of mostly spectral class B, that is, stellar objects of blue color whose spectra are dominated by absorption lines of hydrogen and neutral helium, were investigated from various different perspectives in order to obtain as thorough a picture as possible.

However, while doing so, it became obvious that the applied radiative transfer codes needed some improvements in order to reproduce the observed spectra of the target stars at the highest possible level. Consequently, considerable effort was made in the course of this habilitation project to optimize the modeling of stellar atmospheres and the respective analysis strategy, eventually rendering it one of the best tools to study early-type stars.

The application of this improved analysis methodology to four different objects yielded novel observational insights into the structure and evolution of stars: i) Theoretical predictions for the sizes of the hydrogen-burning cores of early-type stars – and hence for the width of the upper main sequence – depend on the details of convective mixing and differ for different stellar evolution codes. The slowly pulsating B star 18 Peg was shown to bear great potential as respective benchmark object. ii) Almost all theoretical predictions for the evolution of stripped helium cores assume that these stars have thick hydrogen envelopes. A comprehensive investigation of SDSS J160429.12+100002.2, which turned out to be a proto-helium white dwarf stripped by a substellar companion via common-envelope ejection, provided strong indications that this assumption is not always justified and that the mass of the hydrogen envelope should be considered as an additional parameter. iii) The claimed discovery of a massive stellar black hole next to the early-type star LS V+22 25 has led to controversial discussions because such an object would severely challenge our current view of stellar evolution. A quantitative abundance analysis of LS V+22 25, the mass of which is the most critical ingredient when estimating the mass of the unseen black hole, revealed that it is not a massive main-sequence star as originally assumed but a stripped star of considerably less mass, resulting in a much lower mass for the potential black hole. iv) The cores of hydrogen burning stars are usually covered by an opaque envelope, which is why most of our knowledge about them and their energy-generating nuclear processes comes from theoretical modeling or indirect observations, respectively. Based on a combined spectroscopic and asteroseismic analysis, the early-type star γ Columbae was shown to be the stripped pulsating core of a previously much more massive star that is currently in a short-lived post-stripping structural readjustment phase, making it an extremely rare object and thus an exciting test bed for theory.

Another topic that is addressed in this habilitation thesis are high-velocity early-type stars, in particular their most extreme cases, the so-called hypervelocity stars which are potentially gravitationally unbound to the Milky Way. Driven by data from the *Gaia* space mission, the widely accepted paradigm that hypervelocity stars originate in the Galactic center via a slingshot mechanism was disproved, and arguments were brought forward that an as yet unknown or neglected but powerful acceleration mechanism that ejects stars from the Galactic disk must be at work. Close encounters with very massive stars or intermediate-mass black holes in dense star clusters are possible scenarios for it. The observational results obtained in the course of this habilitation project can help to better understand the conditions in these dense stellar environments, for instance, with respect to the formation of massive stars.

1 Introduction

Stars are the fundamental building blocks of all galaxies, including our Milky Way. Owing to interactions with their ambient interstellar medium, they determine the chemical and structural evolution of their host galaxies. A deep knowledge of stellar physics is thus a necessary prerequisite for understanding almost all phenomena in astronomy, from planetary systems to supernova explosions, from galaxy evolution to cosmology. However, unraveling the physical laws that govern the evolution of stars is not an easy task, and it took mankind more than a century to develop a decent theory of how stars work. According to historical reviews by [Arny \(1990\)](#) and [Bahcall \(2000\)](#), major breakthroughs on the long road to understanding the nature of stars were i) the proposal of contraction as power supply and first theories of stellar evolution based on this idea in the middle of the 19th century, ii) stellar models in which heat is transported solely by convection in the early 20th century, iii) the theory of radiative heat transport in the 1920s, iv) Gamow's theory of Coulomb barrier penetration which opened up the possibility of nuclear reactions as underlying source of energy in the 1930s, v) rapid progress in nuclear physics in the middle of the 20th century and the recognition that the fusion of hydrogen to helium releases energy, vi) the presentation of numerical models that consistently account for energy production and energy transfer by M. Schwarzschild in 1958, and vii) the advent of electronic computers which rendered cumbersome hand integration techniques unnecessary.

Although decades ago, it is fair to say that our qualitative understanding of the evolution of isolated stars has not dramatically changed since the 1960s. Nevertheless, steady progress has been made to further improve stellar models, for instance, by making use of the latest atomic input data or by implementing so far ignored physical effects such as stellar rotation. And yet, many open issues remain. For instance, we are still lacking a self-consistent and non-parametric theory of convective energy transport, which is desperately needed to properly model the envelopes of low-mass stars such as the Sun and the cores of more massive stars. Moreover, it became more and more obvious in recent years that many stars are members of binary or even multiple systems in which the stellar components will interact at some point, for instance, via mass transfer, which can lead to evolutionary paths that are completely different from those of single stars. The so-called common-envelope phase, in which a companion star is swallowed by the expanding envelope of its primary star, is certainly one of the least understood stages in stellar binary evolution, and a quantitative description of the underlying hydrodynamic processes is still highly desired. Similarly, indications for atomic diffusion processes via rotational mixing, gravitational settling, or radiative levitation have been observed in stars but are theoretically poorly described.

Apart from the transfer of mass, stars may also interact dynamically, for example, via close many-body encounters such as binary-binary interactions in dense stellar environments ([Poveda et al. 1967](#)) or a supernova explosion disrupting a binary system ([Blaauw 1961](#)). Depending on the details of the encounter and/or the configuration of the involved binary systems, these interactions may result in the ejection of individual components, which are then called runaway stars because they run away from their original place of birth. Runaway stars that travel so fast that they are gravitationally unbound to the Milky Way are commonly referred to as hypervelocity stars (HVSs). Unraveling the origin of these rare objects is particularly interesting because they clearly constitute the outcome of very violent ejection events. The most popular explanation for HVSs is the so-called Hills mechanism ([Hills 1988](#)), which theorizes the tidal disruption of a

binary system by a supermassive black hole. Because the Galactic center is the only place that is known to host such a supermassive black hole, it is the suggested place of origin for many of the HVSSs. All three ejection mechanisms mentioned above have in common that the more massive and the closer the involved objects are, the larger the typical ejection velocity is. Consequently, high-velocity stars probe extreme cases of stellar configurations/environments and thus offer important constraints on stellar evolution theory.

Observations have always been the key drivers for progress in the field of stellar structure and evolution theory. For instance, the launch of space telescopes like *Kepler* (Koch et al. 2010) or *TESS* (Ricker et al. 2016) enabled asteroseismology, that is, the study of the pulsational properties of stars, to become one of the most powerful tools for probing the internal structure of stars and, in this way, to improve our knowledge of stellar evolution by looking at the light curves of stars. Similarly, completed and running large-sky photometric surveys, both ground- and space-based, built up huge databases of stellar flux measurements that range from the ultraviolet over the optical to the infrared, enabling us now to study almost the full spectral energy distribution (SED) of stars. An ongoing space mission that is currently revolutionizing our picture of the Milky Way is the *Gaia* spacecraft (Gaia Collaboration et al. 2016), which measures parallactic distances, positions, and proper motions of more than a billion stars with unprecedented accuracy and precision. Knowing the distance to a star allows for an inference of its fundamental parameters – radius and mass – that is completely independent of stellar models. Consequently, *Gaia* provides unparalleled opportunities to test stellar evolution theory. In addition, the unique quality of *Gaia* astrometry opens the door to a new era in kinematic investigations of runaway and HVSSs, allowing ejection velocities and spatial origins to be determined with sufficient precision to severely challenge longstanding assumptions in the research field.

The goal of this habilitation project is to exploit this new wealth of observational data to obtain as comprehensive a picture as possible of different kinds of early-type stars in order to gain new insights into the nature of these objects. To this end, a proper modeling of stellar atmospheres as well as an objective analysis strategy is necessary. As outlined in Sect. 2, existing techniques and radiative transfer codes have been improved in the course of this work to make them much more appropriate for investigating the spectra of B-type stars, that is, early-type stars whose spectra are dominated by absorption lines of hydrogen and neutral helium. Furthermore, a simple but powerful tool to analyze the SEDs of stars is presented. Exemplary applications of this refined analysis methodology conclude the modeling part. Section 3 then highlights four individual objects, the analysis of which yielded new observational insights into the structure and evolution of stars: i) A slowly pulsating B star as testbed for upper main sequence stellar evolution (18 Peg), ii) a proto-helium white dwarf stripped by a substellar companion via common-envelope ejection (SDSS J160429.12+100002.2), iii) a stripped B-type star in the potential black hole binary LB-1 (LS V+22 25), and iv) a recently stripped, pulsating core of a massive star (γ Columbae). Finally, Sect. 4 shows that the *Gaia* mission is indeed the expected game changer for identifying new high-velocity stars as well as for investigating the kinematic properties of known ones. In particular, it is demonstrated that most HVSSs do not originate in the Galactic center but in the Galactic disk, which rules out the Hills mechanism as acceleration event, and that there is a significant number of disk runaway stars that have ejection velocities in excess of expectations from classical many-body encounters or the supernova binary scenario. This finding constitutes a paradigm shift in the field and indicates that other so-far neglected or unknown ejection events must be at work.

2 Modeling of atmospheres and spectrophotometric analyses

The spectra of early-type stars are usually dominated by hydrogen and helium, both of which exhibit strong absorption lines and are responsible for most of the continuum opacity. Metals, in contrast, are typically only trace elements whose major contribution is the significant number of absorption lines in the far ultraviolet, which, admittedly, is a non-negligible aspect for the computation of stellar atmospheres owing to line blanketing. During my PhD work, I have developed a grid-based global fitting method that facilitates quick and precise determinations of the atmospheric parameters of early-type stars by exploiting these unique spectral properties, in particular, the low density of spectral lines (Irrgang et al. 2014).

2.1 Enhancements of the spectral fitting method

One of the major sources of systematic uncertainty when fitting synthetic to observed spectra is the handling of the continuum. To better cope with this issue, I have added additional features in the meantime that render subjective continuum normalization unnecessary, namely the consideration of telluric transmission models to correct for atmospheric contamination and the possibility to simultaneously fit a cubic-spline continuum or, alternatively, to fit flux-calibrated spectra. The latter option provides access to additional spectral indicators such as the depth and shape of the Balmer jump or the slope of the continuum flux, and is therefore especially useful when working with low-quality spectra that lack, for instance, constraints from ionization equilibria. Several studies in the context of this habilitation project benefited from those improvements in the spectral analysis methodology, for example, the post-doc projects of Marilyn Latour (Latour et al. 2016) and Roberto Raddi (Raddi et al. 2021), for the latter of which I acquired funding by the German Research Foundation, and the PhD thesis of Simon Kreuzer which I co-supervised (Kreuzer 2021).

2.2 Improvements in the computation of synthetic spectra

Besides these advancements in the analysis strategy, significant progress has also been made in the computation of stellar atmospheres and spectra. When dealing with early-type stars, an important aspect to consider is that deviations from local thermodynamic equilibrium (LTE), so-called non-LTE effects, are not negligible owing to the corresponding high photon fluxes and relatively low densities. Consequently, instead of simply applying the Boltzmann and Saha equations, populations numbers have to be obtained by solving the coupled radiative transfer and statistical equilibrium equations, which is numerically much more expensive. A pragmatic compromise between numerical effort and realistic treatment is the so-called hybrid LTE/non-LTE approach discussed by Przybilla et al. (2006) and Nieva & Przybilla (2006, 2007, 2008). Here, the structure of the atmosphere, such as the stratification of temperature and density, is based on line-blanketed, plane-parallel, homogeneous, and hydrostatic LTE-model atmospheres calculated with ATLAS12 (Kurucz 1996). Departures from LTE are then allowed for by calculating atomic population numbers using the DETAIL code (Giddings 1981). Eventually, the SURFACE code (Giddings 1981) is applied to compute the final synthetic spectrum using more sophisticated line-broadening data. Although partly based on LTE concepts, this hybrid method is consistent with full non-LTE calculations for early-type stars (see Nieva & Przybilla 2007;

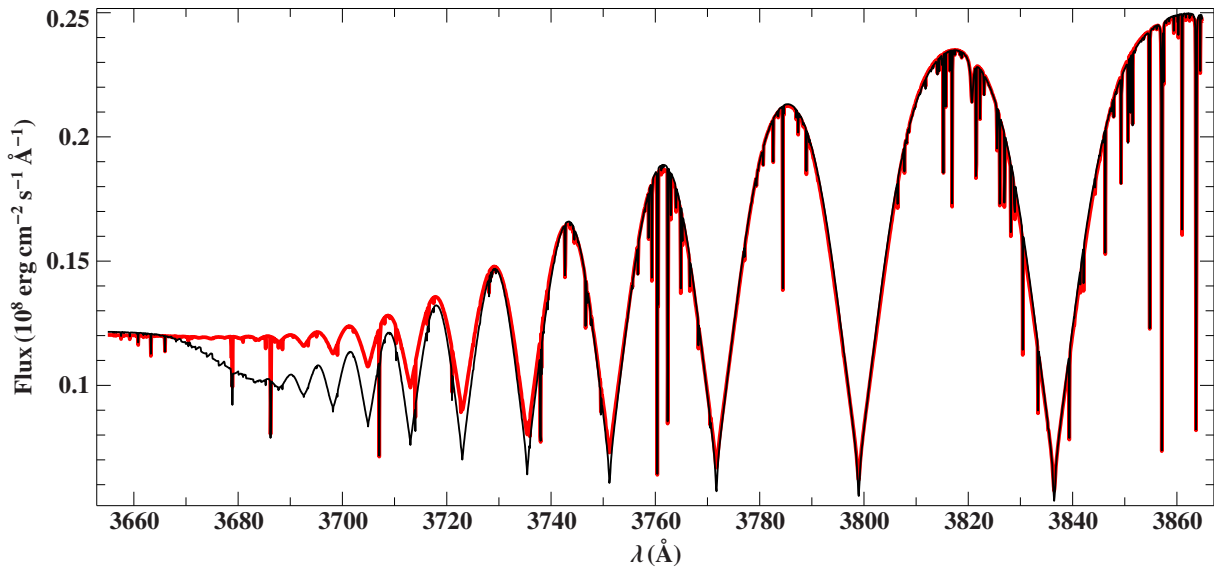


Figure 1. Comparison of synthetic spectra ($T_{\text{eff}} = 12\,000\text{ K}$, $\log(g) = 4.4$, solar composition) calculated with the original ATLAS12 code (thin black line), which uses a non-physical fudge to mimic level dissolution, and my modified version including the occupation probability formalism (thick red line). The proper implementation of this effect allows the region around the Balmer jump, which is an important indicator for the surface gravity, to be exploited for quantitative spectral analysis. From [Irrgang et al. \(2018b\)](#).

[Przybilla et al. 2011](#)) but is considerably faster and, most importantly, is able to handle more detailed representations of model atoms than what is doable with full non-LTE codes. Moreover, instead of relying on pre-calculated opacity distribution functions and hence on prescribed chemical compositions, this hybrid method allows to use the concept of LTE opacity sampling to treat background line opacities (employing the realization of [Kurucz 1996](#)) in all computational steps, making it applicable to almost all kinds of chemically peculiar objects.

However, the hybrid approach suffered from three major issues at the beginning of this habilitation project: i) non-LTE feedback on the atmospheric structure was ignored, ii) level dissolution was not accounted for, and iii) line broadening data for hydrogen and neutral helium were not state-of-the-art. These shortcomings seriously limited the applicability of the resulting models. For instance, the predicted SEDs, most hydrogen and neutral helium lines, and the region around the hydrogen ionization edges such as the Balmer jump were not reliably modeled. These problems have been solved in the meantime (see [Irrgang et al. 2018b](#), appended): i) Non-LTE effects on the atmospheric structure are now considered in the sense that departure coefficients for hydrogen and helium are passed back from DETAIL to ATLAS12 to refine the atmospheric structure iteratively, ii) the occupation probability formalism ([Hummer & Mihalas 1988](#)) for hydrogen and ionized helium – following the description given by [Hubeny et al. \(1994\)](#) – has been implemented to model the dissolution of levels at the series limits, and iii) new Stark broadening tables for hydrogen ([Tremblay & Bergeron 2009](#)) and neutral helium ([Beauchamp et al. 1997](#); [Gigosos & González 2009](#); [Lara et al. 2012](#)) have been incorporated. Figure 1 exemplifies the corresponding improvement in the modeling of the Balmer jump in ATLAS12.

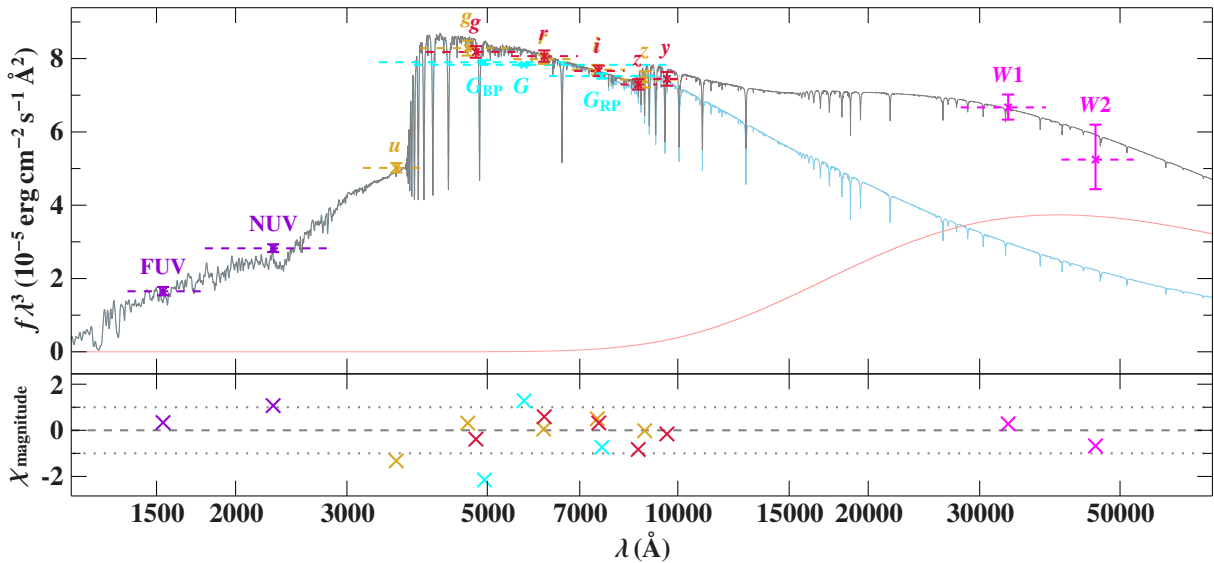


Figure 2. Exemplary comparison of synthetic and observed photometry for an early-type star that exhibits a clear infrared excess, which is modeled here via an additional blackbody component. The *top panel* shows the SED. The colored data points are filter-averaged fluxes that were converted from observed magnitudes (the respective full widths at tenth maximum of the filters are indicated by the dashed horizontal lines), while the solid gray line represents the best fitting ATLAS12 model degraded to a spectral resolution of 6 Å. The flux is multiplied by the wavelength to the power of three to reduce the steep slope of the SED on such a wide wavelength range. The individual contributions of the stellar (light blue) and blackbody (light red) components are shown as well. The panel at the *bottom* shows the residuals, χ , that is, the difference between synthetic and observed magnitudes divided by the corresponding uncertainties. From Irrgang et al. (2021b).

2.3 A simple but powerful tool to study spectral energy distributions

The implementation of non-LTE feedback and level dissolution render ATLAS12 an ideal tool to synthesize realistic SEDs, the study of which can reveal facets of a star that remain otherwise hidden. For example, an infrared excess in the SED of an early-type star could hint at the existence of a cool companion whereas suppressed flux in the ultraviolet is an indicator for strong interstellar absorption. Even without revealing any peculiarities, the SED analysis constitutes a consistency check for spectroscopy and, more importantly, provides easy access to the stellar angular diameter $\Theta = 2R/d$ (R is the radius and d the distance of the star), which can nowadays be combined with parallaxes from *Gaia* to deduce the stellar radius. During this habilitation project, I have written a simple but powerful tool to collect photometric measurements and analyze the resulting SED. To this end, the STILTS software (Taylor 2006) is employed to automatically query basically all major photometric surveys that are publicly available through the Table Access Protocol, most of them via the VizieR online service (Ochsenbein et al. 2000). Synthetic magnitudes, which are calculated via integration of the product of the ATLAS12 surface flux and the corresponding filter transmission curves, are then fitted to these observed flux measurements via χ^2 minimization, see Fig. 2 as well as Heber et al. (2018) for more, yet partly outdated details. Fit-parameters encompass the angular diameter, which acts as distance scaling factor, atmospheric parameters, most notably the effective temperature, and the two quantities

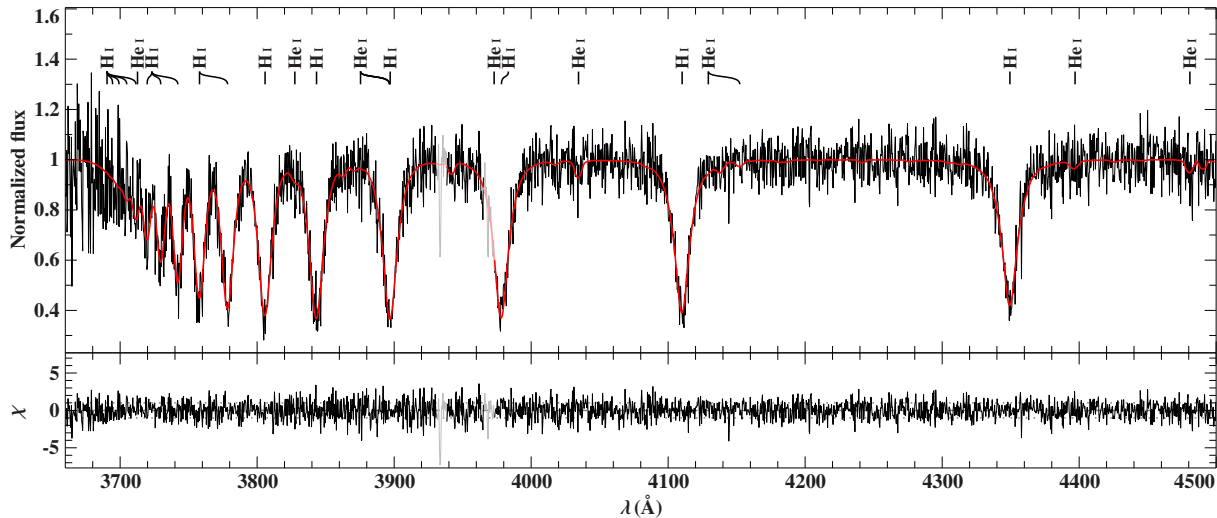


Figure 3. Comparison of a normalized observed spectrum (black, spectral resolution: $\Delta\lambda = 1.2 \text{ \AA}$) with a best-fitting synthetic spectrum computed with the SURFACE code (red), which demonstrates the good reproduction of the Balmer jump. Lines of hydrogen and helium are labeled for reference. Regions contaminated by interstellar Ca II lines were excluded and appear in light colors. Residuals χ are shown in the lower panel. From Irrgang et al. (2018b).

that parameterize interstellar extinction according to Fitzpatrick et al. (2019), namely the color excess $E(44 - 55)$ and the extinction coefficient $R(55)$. Its simple usage, versatility, and the possibility to combine the resulting angular diameter with parallax measurements from *Gaia* to obtain fundamental stellar parameters have caused the tool to be used in various different studies (Németh et al. 2016; Kaplan et al. 2016; Ziegerer et al. 2017; Latour et al. 2018; Schindewolf et al. 2018; Kupfer et al. 2020; Sahoo et al. 2020; Dorsch et al. 2020; Raddi et al. 2021; Baran et al. 2021) and to become a key piece in the analysis strategy of our working group.

2.4 Exemplary applications

All three codes (ATLAS12, DETAIL, SURFACE) do now consistently and realistically reproduce the hydrogen ionization edges, which finally allows for the exploitation of the corresponding spectral ranges in quantitative analyses, see Fig. 3. In the following, a few exemplary studies that made use of these improvements to the codes are highlighted.

2.4.1 Investigation of the ^3He anomaly

The implementation of state-of-the-art Stark broadening tables for hydrogen and neutral helium lines ensures that their spectral shapes are modeled as trustworthy as currently possible. In the course of David Schneider’s MSc and PhD works, which I co-supervised, this paved the way for a quantitative spectroscopic study of the enhancement of the ^3He isotope in subluminescent B-type stars (Schneider et al. 2018, appended). This ^3He anomaly, which was already observed in late B-type main-sequence (MS) stars, blue horizontal branch (BHB) stars, and subdwarf B (sdB) stars, is thought to be the result of atomic diffusion processes, that is, the interplay between gravitational settling and radiative levitation, which causes ^4He to settle more quickly than the

lighter ^3He , hence leading to an enrichment of the latter. Although this balance is conceptually simple to grasp, the existing theories to describe it seem to be too simplistic because they are at odds with observations. To improve our theoretical understanding of atomic diffusion, it is thus vital to provide further guidance by observations. We therefore analyzed high-quality spectra of 13 subluminescent B stars that show the ^3He anomaly (three BHBs, eight sdBs, and two sdBs that were newly discovered to show this peculiarity) to determine their atmospheric parameters and isotopic helium abundances. Because the presence of the ^3He isotope causes the shape of the helium lines to be distorted or shifted depending on the isotopic abundance ratio and on the specific line under consideration, it was essential for this investigation that the underlying line profiles were modeled as reliably as possible to avoid any misinterpretation. Apart from providing accurate positions of the program stars in the Kiel diagram, which is crucial to identify those stages in stellar evolution at which diffusion occurs, we also found indications for vertical helium stratification in three sdB stars. This phenomenon has been seen in other peculiar B-type stars, but was found for the first time for sdBs.

2.4.2 High-precision quantitative abundance studies

Owing to the above-mentioned improvements, the codes are now able to reproduce almost the entire optical spectrum of early-type stars with high fidelity, see Fig. 4. This is very advantageous in the context of quantitative abundance studies, which are often essential to unravel the nature of stars, because it allows basically all spectral indicators to be exploited in order to simultaneously infer atmospheric parameters and chemical abundances with high precision and accuracy.

For instance, based on a differential abundance analysis with respect to the nearby reference star HD 137366, we were able to conclude that the distant B-type star PG 1610+062 is actually a young MS star (Irrgang et al. 2019, appended). This is remarkable because PG 1610+062 is currently located well above the Galactic disk, that is, far away from the star-forming regions of the Milky Way. The subsequent kinematic investigation revealed that PG 1610+062 is one of the most extreme disk runaway MS stars known to date. See Sect. 4.3.2 for further details.

Another example that demonstrates the importance of proper quantitative spectral analyses for unraveling the nature of objects is the controversial discussion about the recently claimed discovery of a massive stellar black hole in the binary system LB-1, which will be covered in more detail in Sect. 3.3. Here it suffices to mention that a high-precision abundance study based on our new models provided strong evidence for the idea that the stellar component in the system is actually not a normal MS B-type star but a stripped helium star, which severely lowers the inferred mass of the potential black hole (Irrgang et al. 2020b, appended). Moreover, our revised model spectra served as internal cross-check in the course of the analysis of follow-up low-resolution *Hubble* spectra of LB-1 (Lennon et al. 2021, appended).

2.4.3 Computation of a grid of spectra for subdwarf B- and O-type stars

A further major application of the revised codes is the computation of an extensive grid of spectra that covers subdwarf B- and O-type stars, which has been utilized in the studies by Silvotti et al. (2021) and Schaffenroth et al. (2021) as well as in several other projects that are not yet published.

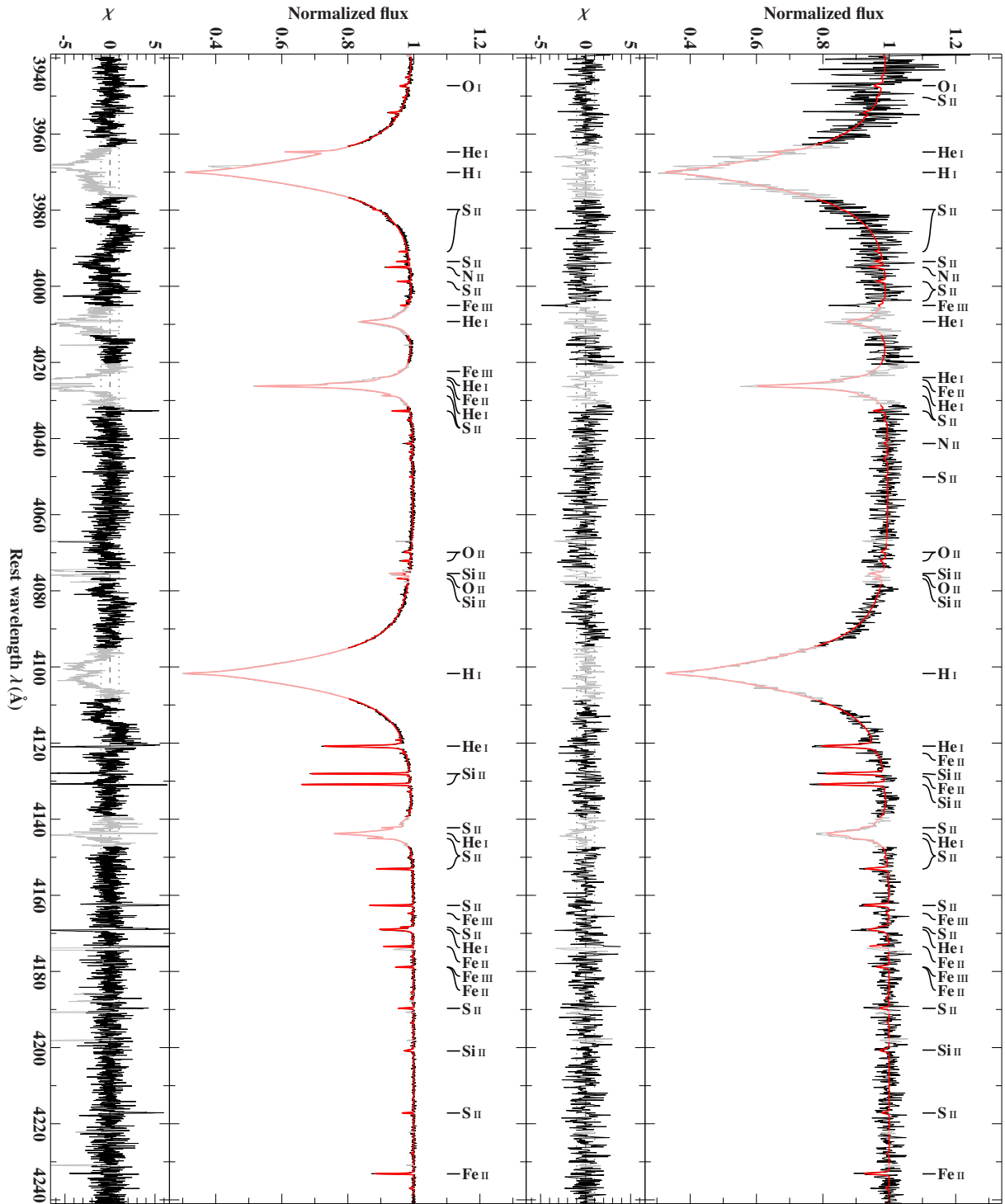


Figure 4. Comparison of best-fitting model spectrum (red line) with normalized observed spectrum (black line) for HD 137366 (*left*, spectral resolution: $\lambda/\Delta\lambda \approx 48\,000$, signal-to-noise ratio: $S/N \approx 470$) and PG 1610+062 (*right*, $\lambda/\Delta\lambda \approx 8000$, $S/N \approx 60\text{--}110$). Light colors mark regions that have been excluded from fitting (e.g., due to data reduction artifacts, insufficient correction of telluric lines, or the presence of features that were not properly included in the models at the time of the analysis such as state-of-the-art helium line-broadening data). For the sake of clarity, only the strongest of the lines used in the analysis are labeled. From [Irrgang et al. \(2019\)](#).

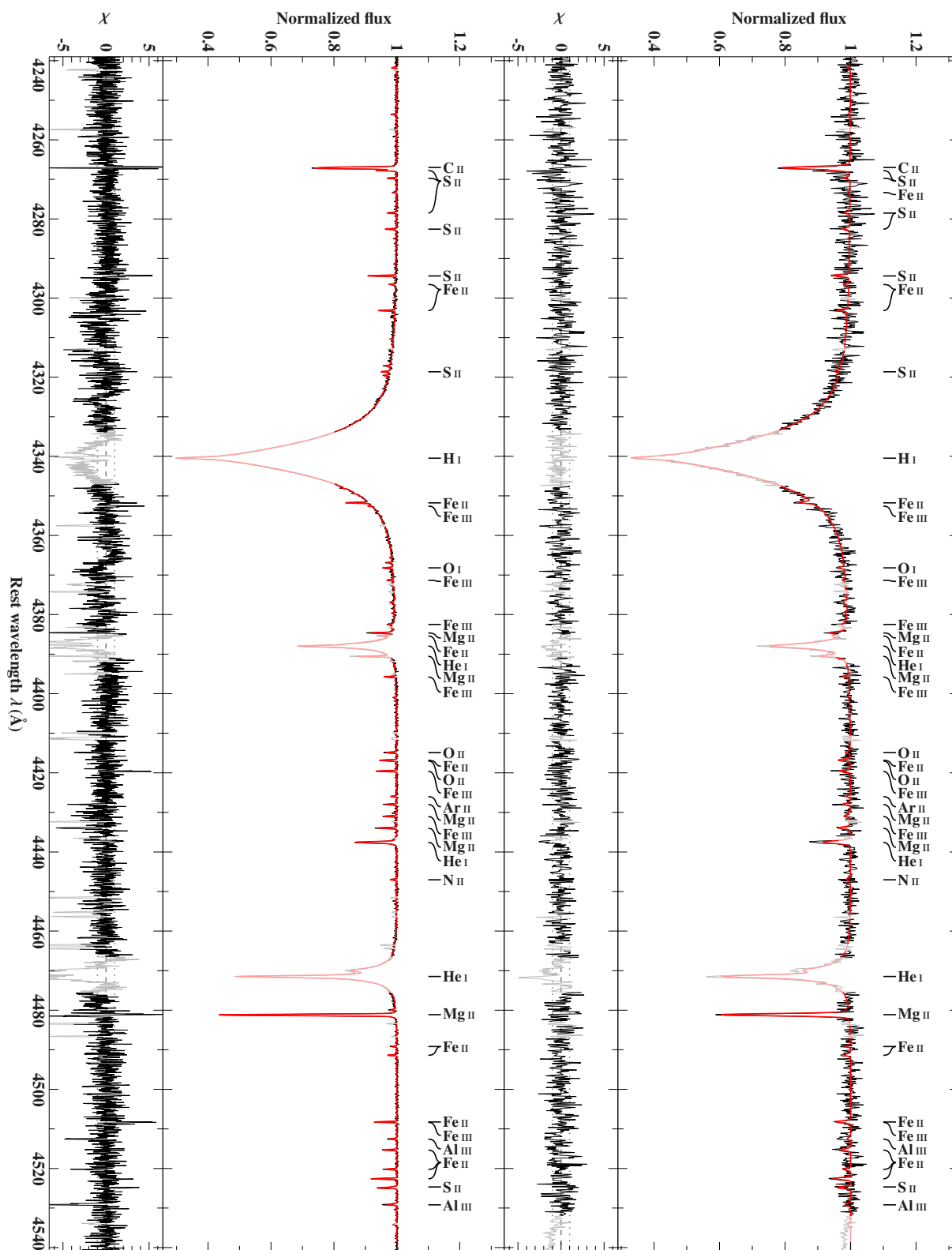


Figure 4. Continued.

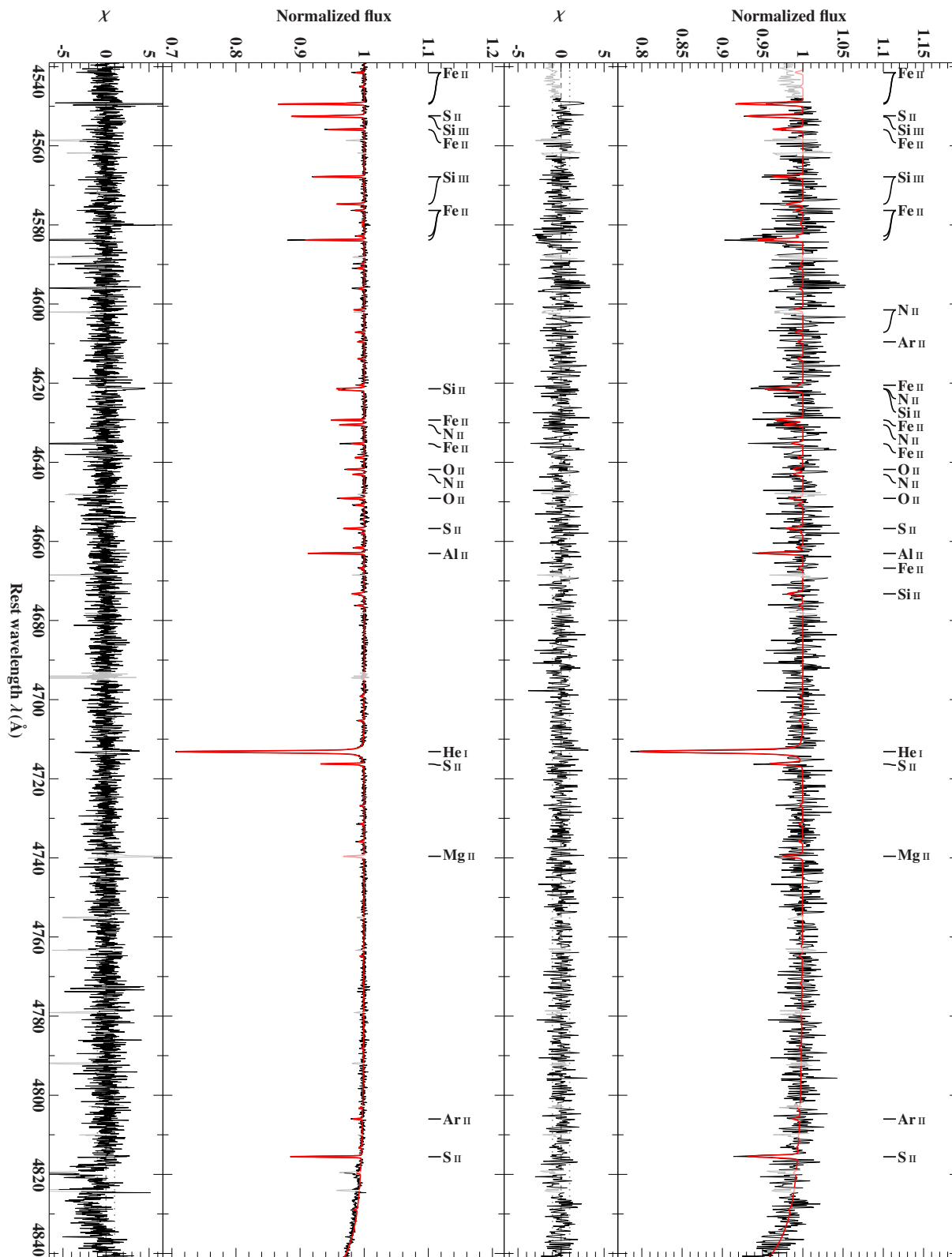


Figure 4. Continued.

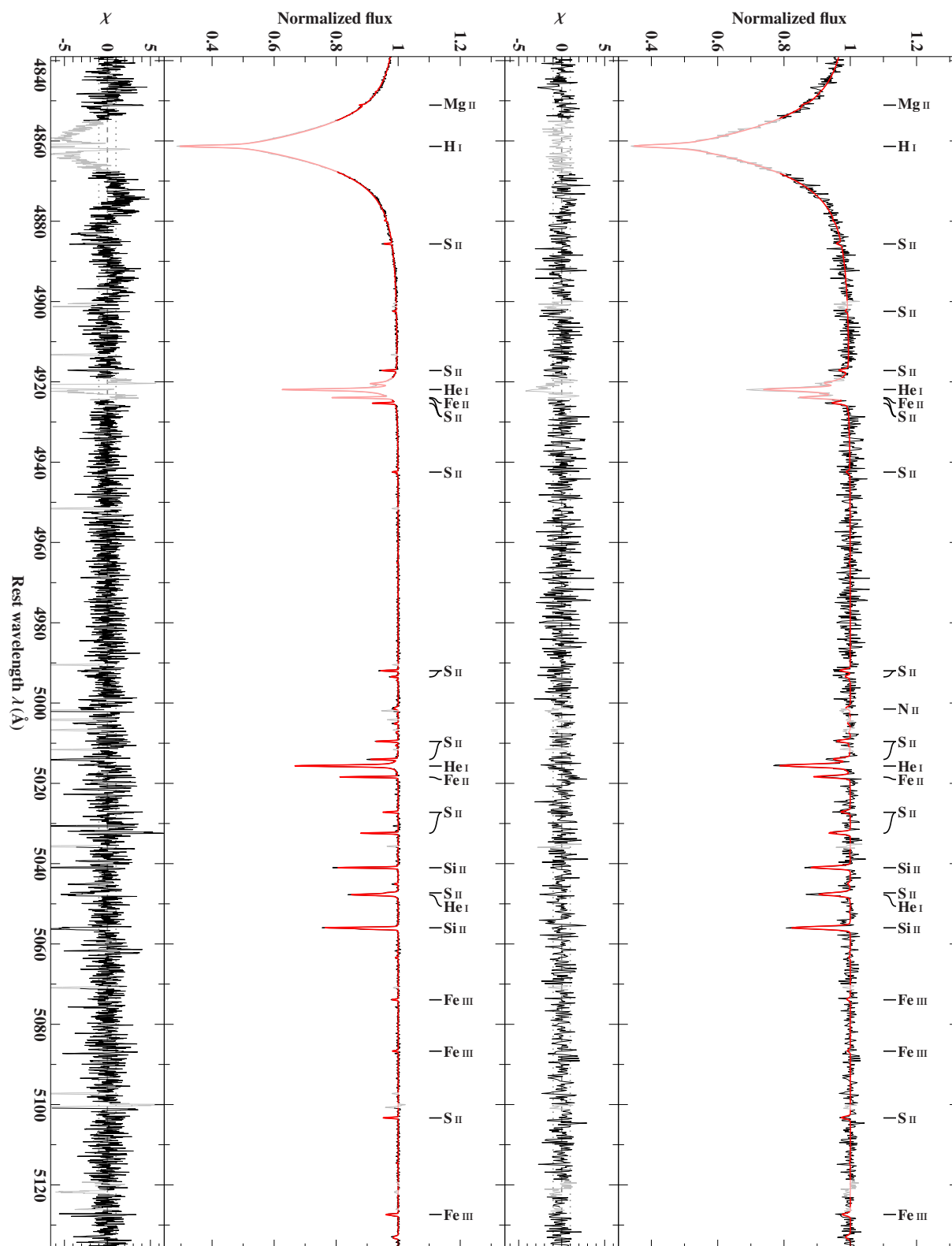


Figure 4. Continued.

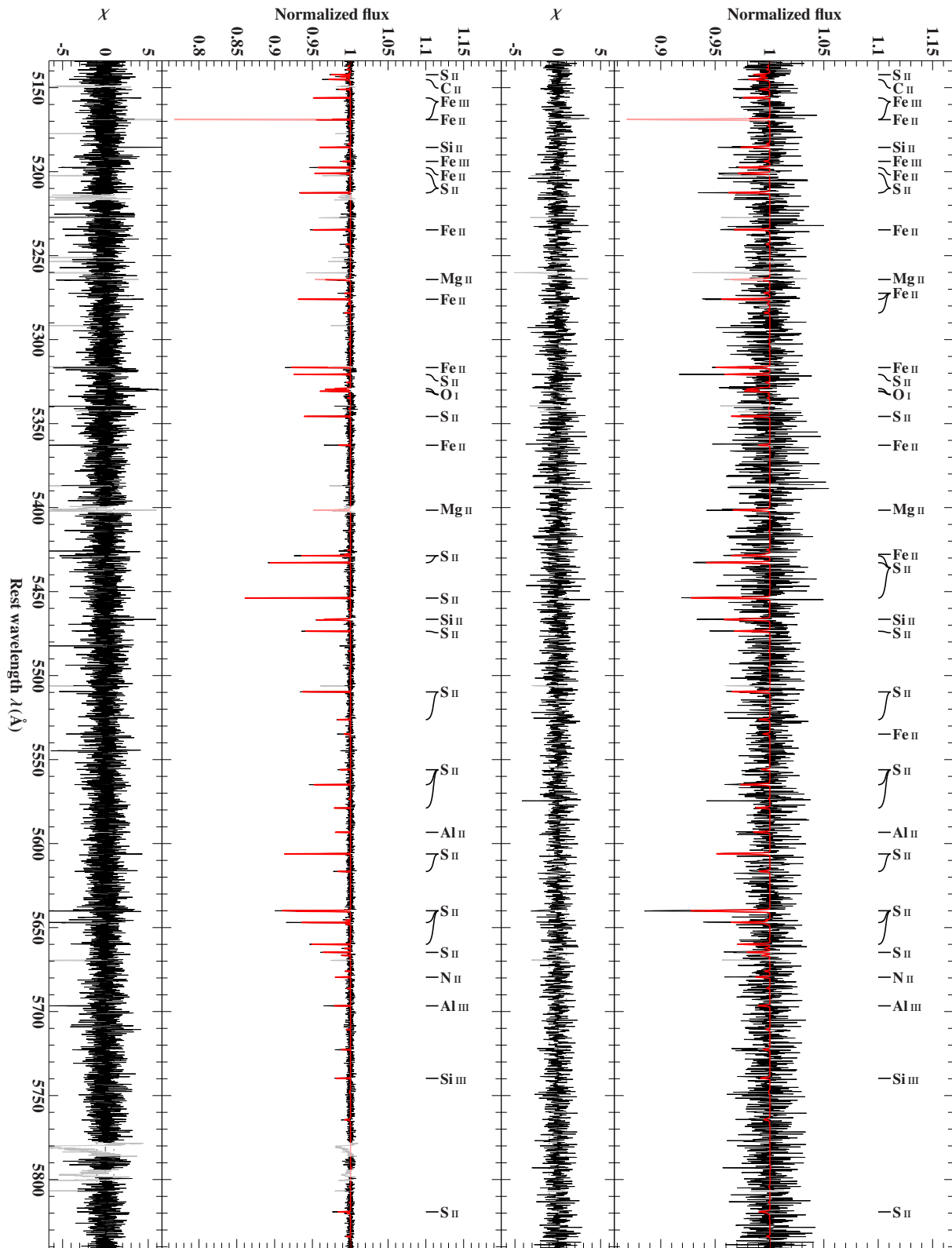


Figure 4. Continued.

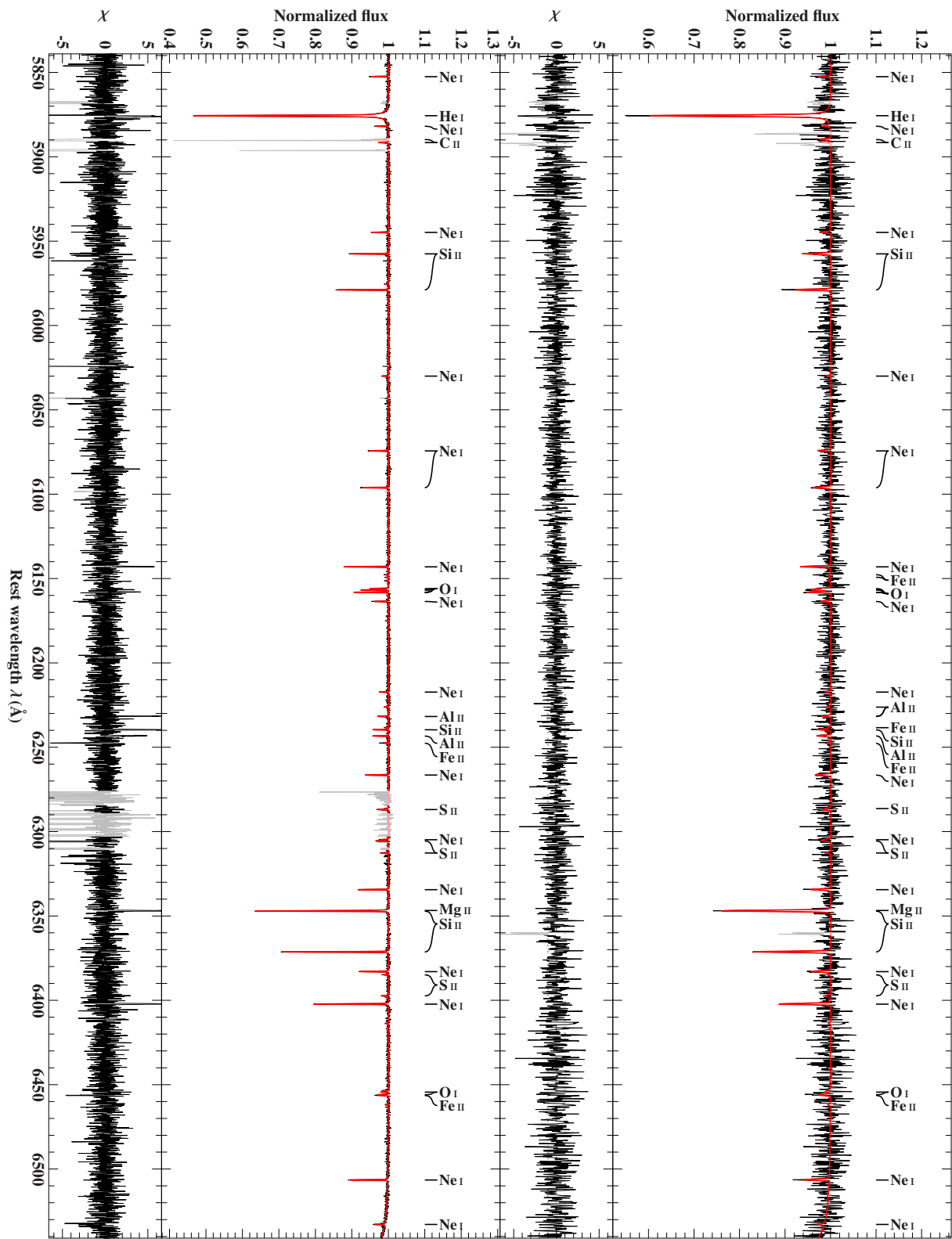


Figure 4. Continued.

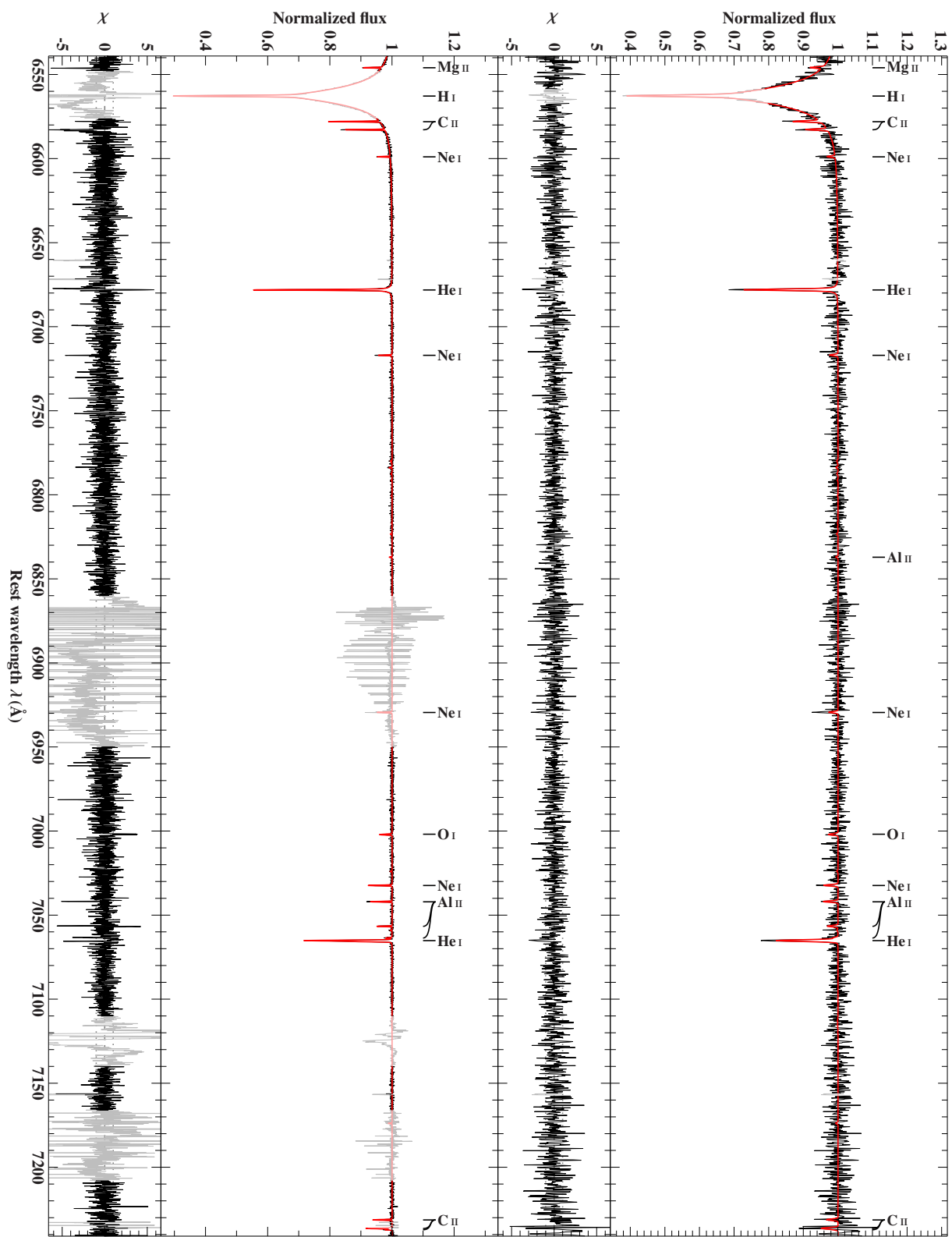


Figure 4. Continued.

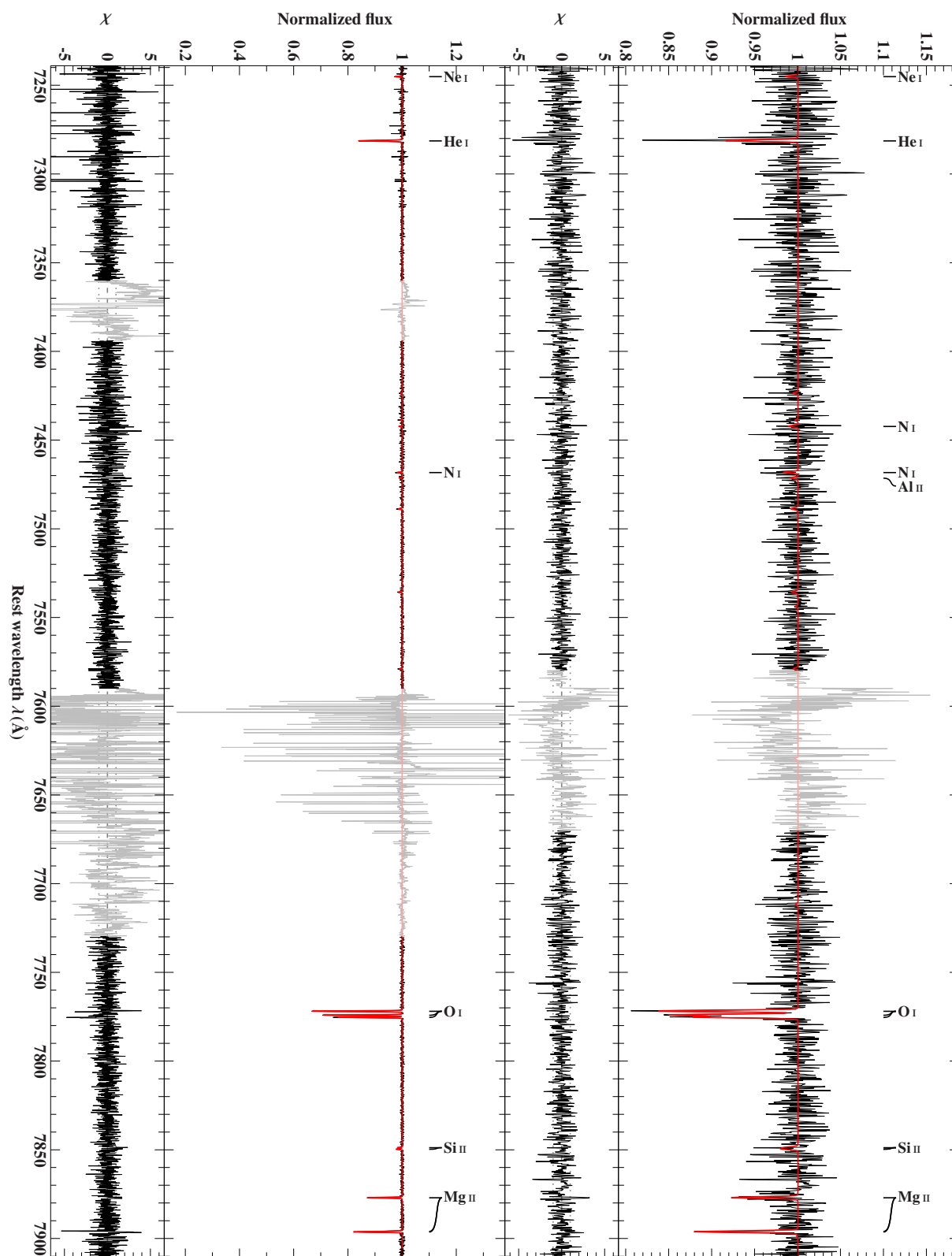


Figure 4. Continued.

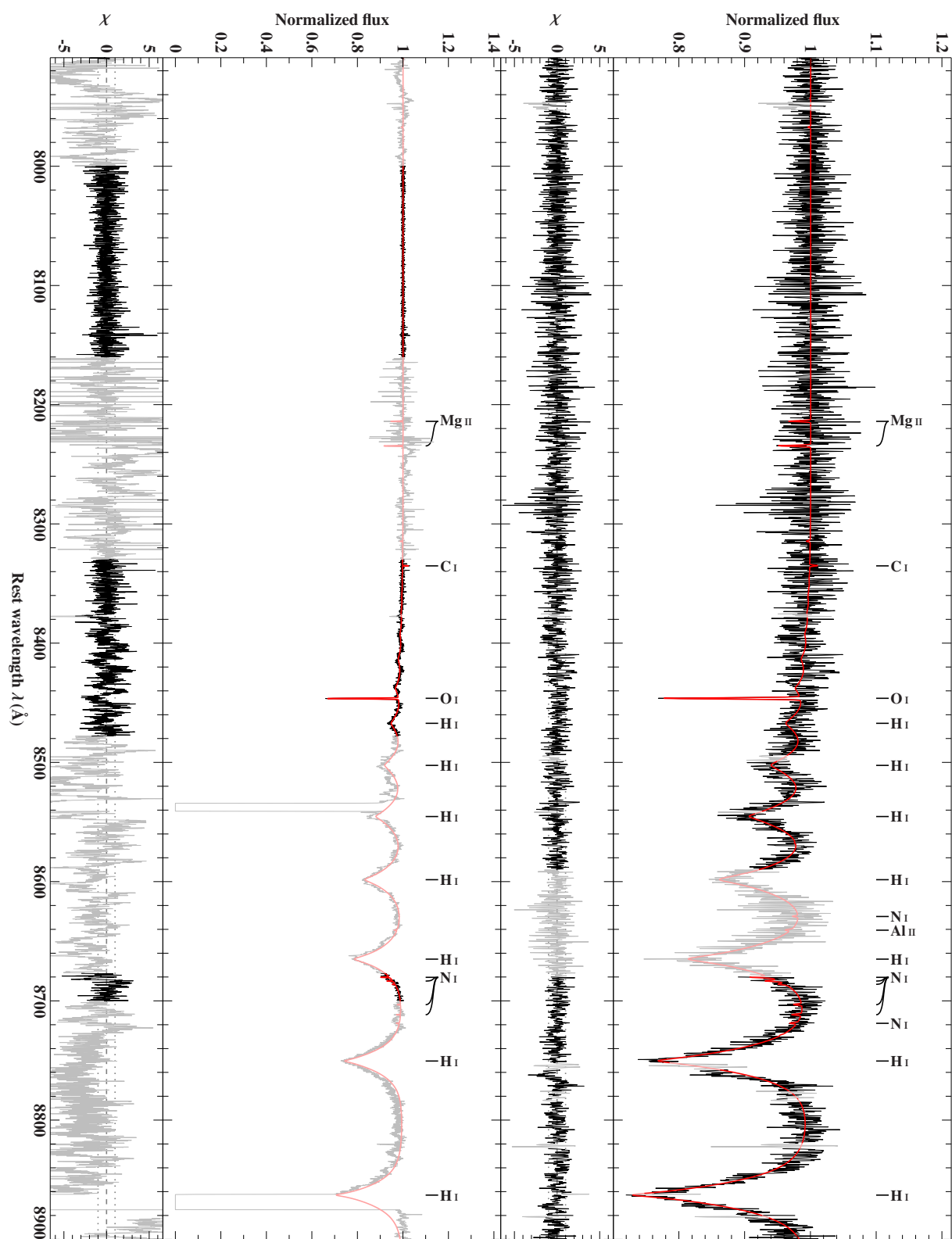


Figure 4. Continued.

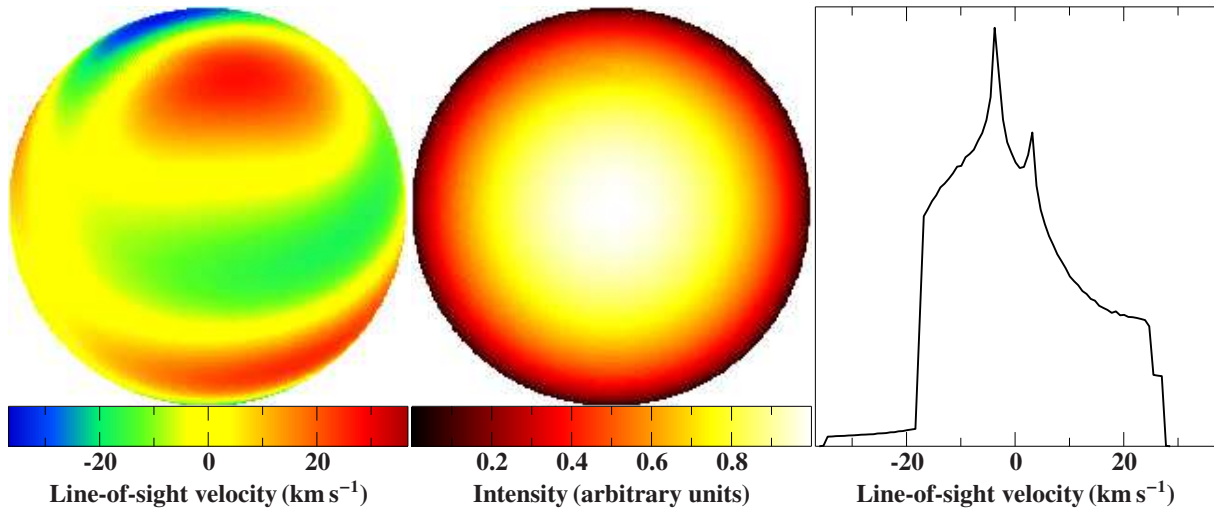


Figure 5. Snapshot of a non-radial stellar pulsation of a non-rotating star seen under an inclination of 45° with respect to its pulsational axis. The left and middle panels display the projected stellar disk color coded with the line-of-sight velocity or the intensity, respectively. The right panel shows the line-broadening Doppler profile resulting from disk integration of the velocity field using the intensity map as weighting factor. See [Irrgang et al. \(2016\)](#) for more, yet partly outdated details on the underlying model.

3 Constraining stellar models via pulsating and/or stripped stars

Studying the pulsational properties of stars has become a hot topic because it is a powerful tool for probing the internal stellar structure and, in this way, to improve our knowledge of stellar evolution (see, e.g., [Aerts et al. 2010](#)). Pulsating early-type stars are typically driven by an “opacity bump” mechanism that excites non-radial oscillation modes. The observational signatures of this kind of stellar pulsations are periodic brightness variations in the light curve of the object as well as temporal distortions in the spectral line profiles. While the light-curve analysis is the standard tool of asteroseismology, it can also be very rewarding to quantitatively study the line-profile distortions because this approach provides constraints on pulsational parameters that are not accessible otherwise. In the course of this habilitation project, I have developed a tool that allows the spectral line-broadening of non-radial pulsations to be modeled, see Fig. 5, which was then successfully applied in the analyses of a slowly pulsating B (SPB) star (see Sect. 3.1) and of a recently stripped, pulsating core of a massive star (see Sect. 3.4).

B-type spectra can be observed for stars of very different evolutionary stages. The most common ones are young, massive ($\gtrsim 2.5 M_\odot$) MS stars. However, the much less massive ($\sim 0.47 M_\odot$) and smaller sdBs show relatively similar spectra. Most of them are likely core helium-burning stars located on or somewhat evolved away from the horizontal branch. In addition, even less massive ($\sim 0.2\text{--}0.47 M_\odot$) helium stars, which are direct progenitors of helium white dwarfs, can show B-type spectra for a period of time ($\sim 10^6\text{--}10^7$ yr; e.g. [Driebe et al. 1998](#)) during their evolution (e.g. [Latour et al. 2016](#)). One common feature of most low-mass B-type stars is that they are helium stars, which is difficult to explain using evolutionary scenarios involving only single stars. Instead, they are assumed to be the exposed cores of low-mass stars that have lost most of their hydrogen envelope during their ascension of the red giant branch,

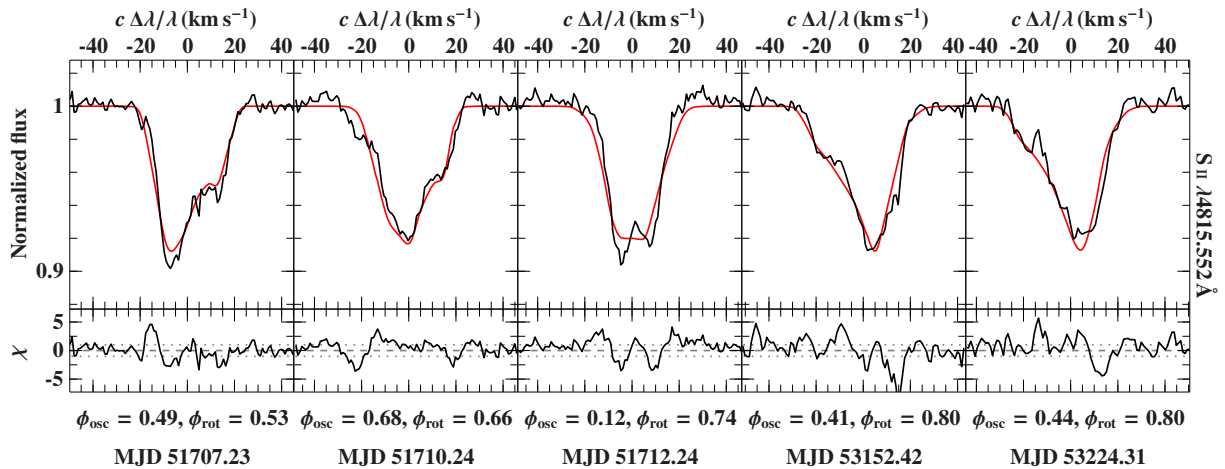


Figure 6. Spectral modeling of the pulsationally driven line-profile distortions of the slowly pulsating B star 18 Peg for five epochs and one exemplary sulfur line: the observations are indicated by a black line, the model by a red one, and the quality of the fit by the residuals χ . From [Irrgang et al. \(2016\)](#).

either well before or at the moment at which helium-burning starts in their core. The stripping is done either by stable Roche lobe overflow to a companion star or via unstable common-envelope ejection. Stripped helium stars with masses higher than $\sim 0.47 M_{\odot}$ are also predicted by binary evolution models ([Götberg et al. 2018](#)), but are expected to be much rarer and only very few of them have been observed so far. Two new such stars are presented in the following (see Sect. 3.3 and 3.4). Furthermore, the discovery of an unevolved proto-helium white dwarf that was stripped by a substellar companion is reported (see Sect. 3.2).

3.1 A pulsating B star as testbed for main sequence stellar evolution

The bright ($G = 5.96$ mag) B-type star 18 Peg had never received much attention itself but had rather been utilized very often as a telluric standard or as a background source to investigate the chemical composition of the interstellar medium. However, based on the resulting wealth of high-quality archival data, we discovered that the star exhibits small changes in brightness as well as distortions of its line profiles on a timescale of a few days, see Fig. 6. A careful modeling of these temporal variations showed that they can be explained by 18 Peg being a member of the rare class of SPB stars. This finding was particularly interesting because 18 Peg is already quite evolved, in fact, it turned out to be one of the most evolved SPB stars currently known. Pulsation models predict that SPB stars are MS stars because their non-radial gravity modes are strongly damped in the interiors of post-MS stars. Consequently, 18 Peg provides a tight lower limit for the width of the upper MS (see Fig. 7), the prediction of which is a long-standing challenge in stellar evolution theory. The reason for this is that the hydrogen-burning cores of upper MS stars are convective. The predicted core sizes thus depend on the treatment of convection, which, in most cases, relates to the parameterization of the mixing-length theory, in particular on the empirical calibration of the overshooting parameter. Despite decades of discussions, the precise value of this parameter is still unknown and further observational constraints are required to gauge it. Our investigation showed that 18 Peg bears the potential to provide such a benchmark ([Irrgang et al. 2016](#), appended). In this context, it is worthwhile to mention that I

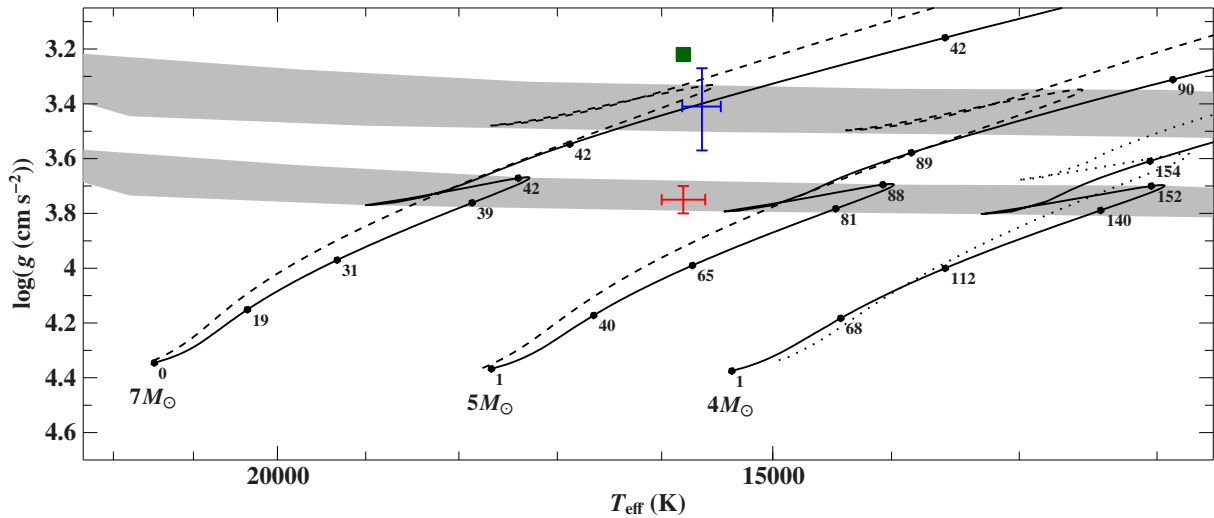


Figure 7. Position of 18 Peg in the Kiel diagram based on spectroscopy (Nieva & Przybilla 2012, red error bars), photometry (blue error bars), and pulsational line-profile modeling (green square; T_{eff} taken from spectroscopy). Overlaid are evolutionary tracks for non-rotating stars of solar metallicity and different initial masses by Brott et al. (2011, dashed lines) and Ekström et al. (2012, solid lines). The numbers next to the black filled circles give the evolutionary age in Myr. The gray-shaded areas highlight the transition region between MS and post MS for the two different sets of models, illustrating their contradictory predictions for the width of the MS. The MS nature of 18 Peg sets a lower limit on the vertical position of this transition region. From Irrgang et al. (2016). Note that a spectral reanalysis based on the revised strategy outlined in Sect. 2 yields $\log(g) = 3.59 \pm 0.05$ instead of $\log(g) = 3.75 \pm 0.05$, i.e., a much better match between spectroscopy and photometry as well as a tighter lower limit on the width of the MS.

was also involved in a study of the runaway β Cep pulsator PHL 346 (Handler et al. 2019), which demonstrated that pulsating runaway stars can also serve as vital probes to better understand the interior structure of massive stars.

3.2 A proto-helium white dwarf stripped via common-envelope ejection

SDSS J160429.12+100002.2, a rather faint ($G = 17.13$ mag) B-type star of relatively high Galactic latitude ($b = +41.5$ deg), was initially considered to be a candidate hypervelocity star. However, a quantitative analysis of multi-epoch follow-up spectra revealed that the target is actually a short-period single-lined spectroscopic binary system. Moreover, combining constraints from astrometry, orbital motion, photometry, and spectroscopy, the visible component in this system turned out to be an unevolved proto-helium white dwarf that was stripped by a substellar companion through common-envelope ejection. This proved to be an interesting discovery for stellar evolution theory for two reasons: i) Our study was one of the very rare cases that have allowed for a comprehensive abundance analysis of a proto-helium white dwarf. The abundances of He, C, N, O, Ne, Mg, Al, Si, S, and Ca in the atmosphere of SDSS J160429.12+100002.2 are subsolar by factors from 3 to more than 100, while Fe is enriched by a factor of about 6. This peculiar chemical composition pattern is indicative of ongoing atomic diffusion processes and can hence serve as observational anchor point for

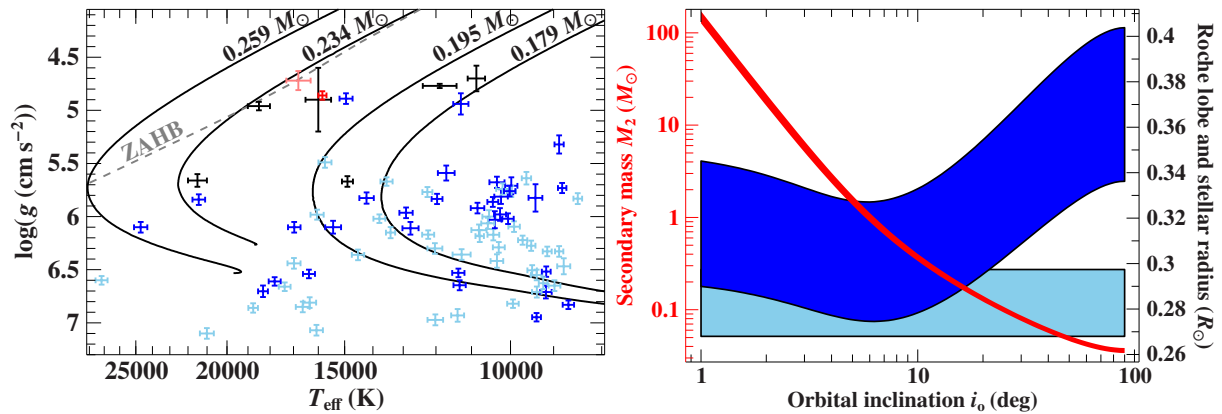


Figure 8. *Left panel:* Position of SDSS J160429.12+100002.2 (dark red 1σ error bars) in the Kiel diagram. The black lines are standard evolutionary tracks for stripped helium cores from [Driebe et al. \(1998\)](#) labeled with their respective masses. This comparison suggests that the star is a proto-helium white dwarf of $M_1 = 0.21 \pm 0.01 M_\odot$ that has shrunk by a factor of about 8.5 since the stripping event. *Right panel:* Mass and Roche lobe radius as a function of orbital inclination. *Left ordinate (red):* Mass of the unseen companion, M_2 , as a function of the orbital inclination, i_o , assuming $M_1 = 0.21 \pm 0.01 M_\odot$ for the proto-helium white dwarf. *Right ordinate (black-rimmed blue-shaded curves):* Comparison of the Roche lobe radius of the proto-helium white dwarf (dark blue) and the respective stellar radius (light blue) following from $M_1 = 0.21 \pm 0.01 M_\odot$ and from the spectroscopically inferred surface gravity. Physical conditions are met when the light blue band is below the dark blue band, that is, when the star is smaller than its Roche lobe radius. This figure demonstrates that the star is currently already close to filling its Roche lobe and thus could not have been considerably larger in the past, which is at odds with predictions from standard evolutionary tracks. From [Irrgang et al. \(2021b\)](#).

studying the details of those complex processes. ii) Standard evolutionary tracks for stripped helium cores predict post-stripping stellar radii that are too large to be consistent with the current orbital configuration of SDSS J160429.12+100002.2, see Fig. 8, thus making the object a promising test bed for theory. Motivated by the Roche-lobe overflow scenario, all of those standard evolutionary tracks are computed for thick hydrogen envelopes. However, this approach may not be valid for systems that underwent a common-envelope phase, as we proposed for SDSS J160429.12+100002.2. Following [Calcaferro et al. \(2018\)](#), we argued that models with thin hydrogen envelopes would probably resolve this inconsistency because they predict smaller stellar radii. Consequently, the thickness of the hydrogen envelope should be considered as an additional parameter in the spectroscopic mass and age determinations of (proto-)helium white dwarfs in post common-envelope systems ([Irrgang et al. 2021b](#), appended).

3.3 A stripped B-type star in the potential black hole binary LB-1

Another intriguing target is the B-type star LS V+22 25, that is, the visible component in the potential black hole binary system LB-1, which was already briefly mentioned in Sect. 2. This system has become famous for possibly hosting a massive ($M_{\text{BH}} = 68_{-13}^{+11} M_\odot$) stellar black hole in the Galactic solar neighborhood, which led to controversial discussions because such a discovery would severely challenge our current view of stellar evolution (see, e.g., [Liu et al. 2019](#); [Eldridge et al. 2020](#); [Groh et al. 2020](#); [Belczynski et al. 2020](#)). A crucial aspect for the de-

termination of the mass of the unseen black hole is the precise nature of its visible companion. Because stars of different mass can exhibit B-type spectra during the course of their evolution, it was essential to obtain a comprehensive picture of LS V+22 25 to unravel its nature and, thus, its mass. To this end, we studied its SED and performed a quantitative spectroscopic analysis that included the determination of various elemental abundances, which revealed that LS V+22 25 is not an ordinary MS B-type star as assumed previously. The derived abundance pattern exhibits heavy imprints of the CNO bi-cycle of hydrogen burning, that is, He and N are strongly enriched at the expense of C and O, which indicates that LS V+22 25 is a stripped helium star. Combining our photometric and spectroscopic results with the parallax measurement from *Gaia*, we inferred a stellar mass of $1.1 \pm 0.5 M_{\odot}$. Based on the binary system's mass function, this yielded a minimum mass of $2\text{--}3 M_{\odot}$ for the compact companion, which implied that it may not necessarily be a black hole but a massive neutron- or MS star (Irrgang et al. 2020b, appended). Based on much more and much better optical spectra, these results were later on confirmed by Shenar et al. (2020) who used spectral disentangling to demonstrate that the putative compact object in the system is actually a rapidly spinning Be star of similar brightness than LS V+22 25. Rapid rotation and dilution caused its photospheric absorption lines to remain hidden in individual spectra, which is why it was not found before. Finally, using low-resolution spectra from *Hubble* that cover the entire range from the ultraviolet to the near-infrared, we slightly refined the Shenar et al. model (Lennon et al. 2021, appended).

3.4 A recently stripped, pulsating core of a massive star

The fourth and last target of discussion is again a very bright ($G = 4.32$ mag) object that had not been well studied before although high-quality spectra had been publicly available. Our quantitative spectral analysis of those archival data revealed that γ Columbae, which at first glance looks like a typical star in the solar neighborhood, is anything else but normal. While the inferred atmospheric parameters indicated that the star may just be an ordinary subgiant of spectral class B, a standard evolutionary history could be excluded right away on the basis of the derived surface abundance pattern, which exhibits heavy imprints of the CNO bi-cycle of hydrogen burning. Interestingly, neither hydrodynamic mixing of core fusion products with pristine material in the stellar envelope nor the stripping off the envelope by powerful winds offered a satisfactory explanation for the results of our spectral analysis. Instead, because the observed mass fractions of those chemical elements that are affected by the CNO cycle nicely match the predicted abundances of a $4\text{--}5 M_{\odot}$ core of a $12 M_{\odot}$ stellar model close to the end of central hydrogen fusion (see Fig. 9), we argued that γ Columbae is the exposed core of a massive star that has been stripped via common-envelope ejection. The position of the star in the Hertzsprung-Russell diagram would then imply that it is currently in a short-lived post-stripping structural readjustment phase (see Fig. 10), rendering it an extremely rare object. On top of that, γ Columbae shows temporal variations in its light curve and in its spectral line profiles that are very similar to those of SPB stars except for its main oscillation period, which is several years instead of a few days. The discovery of this extraordinary object paves the way to obtain invaluable insights into the physics of both single and binary stars with respect to nuclear astrophysics and common-envelope evolution, for instance, via detailed asteroseismic studies in the future. In particular, it provides unique observational constraints on the structure and evolution of stripped envelope stars (Irrgang et al. 2022, appended).

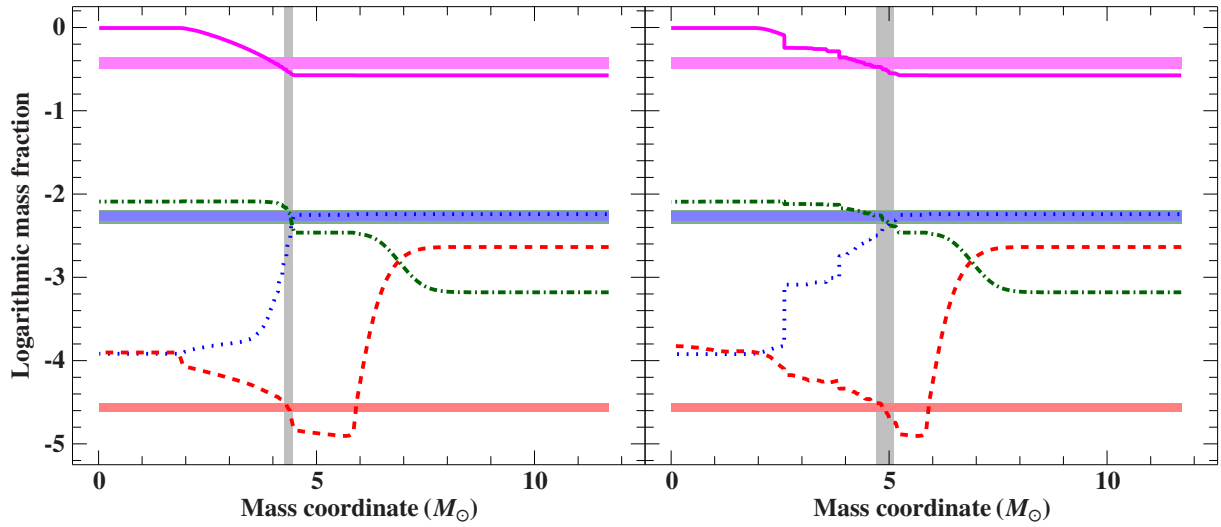


Figure 9. Comparison between observed abundances and theoretical predictions for the depth-dependent chemical composition in a massive star. Logarithmic mass fractions for He (magenta solid line), C (red dashed line), N (green dashed-dotted line), and O (blue dotted line) are plotted as a function of interior mass for a non-rotating stellar model (Ekström et al. 2012) with solar metallicity and initial mass of $12 M_{\odot}$ at two moments shortly after the end of central hydrogen fusion (*left*: age $\tau = 15.48$ Myr, radius $R = 8.6 R_{\odot}$; *right*: $\tau = 15.53$ Myr, $R = 16.1 R_{\odot}$). The observed surface abundances of γ Columbae, whose 99% confidence intervals are represented by colored horizontal bars, are well reproduced by the model for interior masses marked by gray vertical bars, which indicates that the object could be the stripped 4–5 M_{\odot} core of a $12 M_{\odot}$ star. From Irrgang et al. (2022).

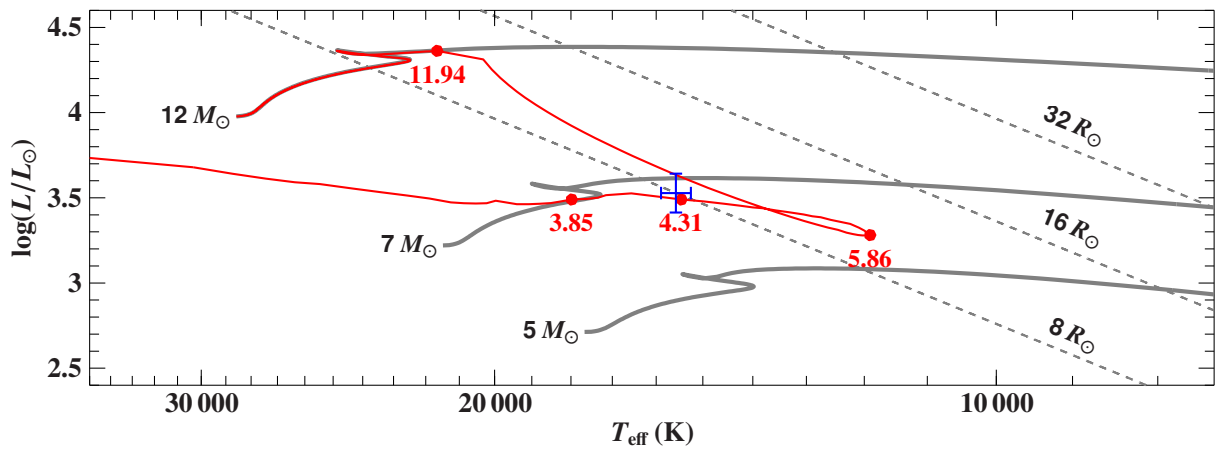


Figure 10. Stellar evolution in the Hertzsprung-Russell diagram. The evolution of effective temperature T_{eff} and stellar luminosity L for a non-rotating stellar model with solar metallicity and initial mass of $12 M_{\odot}$ – with an additional artificial mass loss of $1.29 \times 10^{-3} M_{\odot} \text{ yr}^{-1}$ switched on shortly after the end of central hydrogen fusion – is shown (red solid line; the numbers next to the points indicate the mass in M_{\odot} at that point in time). The position of γ Columbae (blue; error bars are 99% confidence intervals), evolutionary tracks for non-rotating single stars of solar metallicity (Ekström et al. 2012, gray solid lines), and loci of constant radius (gray dashed lines) are shown for reference. The stripped model with a respective mass of $4.31 M_{\odot}$ exhibits surface abundances as indicated by the gray vertical bar in the left panel of Fig. 9 and is thus not only able to reproduce γ Columbae’s stellar parameters (mass, radius, and luminosity) but also its observed mass fractions for He, C, N, and O. From Irrgang et al. (2022).

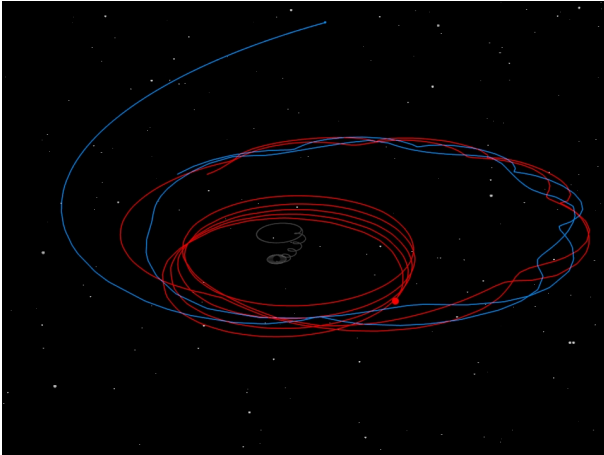


Figure 11. Illustration of the Hills mechanism. The tidal disruption of an initially bound binary system (red and blue trajectories) by a massive black hole (gray trajectory) can accelerate one component (blue) at the expense of the other component's (red) potential energy. According to [Hills \(1988\)](#), ejection velocities up to a few thousand kilometers per second are possible with this slingshot mechanism. An animated version of this figure is available [online](#).

4 Origin of hypervelocity and runaway stars

Driven by the unprecedented astrometric quality offered by the *Gaia* space mission, we embarked on a project that aimed at unraveling the nature and origin of known high-velocity stars as well as at finding new ones. This led to a series of papers in the course of this habilitation work whose results are briefly summarized in the following.

4.1 Hypervelocity stars (HVSs)

Hypervelocity stars travel so fast that they are potentially unbound from the Galaxy. When they were discovered serendipitously more than fifteen years ago ([Brown et al. 2005](#); [Hirsch et al. 2005](#); [Edelmann et al. 2005](#)), the so-called Hills mechanism ([Hills 1988](#)) was readily accepted as a viable ejection mechanism. According to Hills, the supermassive black hole at the Galactic center acts as a slingshot by tidally disrupting binary systems (see Fig. 11 as well as [Brown 2015](#) for a review). Because the first HVS was found to be a late B-type MS star, a wide-field spectroscopic survey was initiated that targeted stars of similar spectral type and mass ($2.5\text{--}4 M_{\odot}$). After surveying no less than 12 000 square degrees of the northern sky, 42 bound and unbound candidate HVSs of late B-type have been discovered ([Brown et al. 2014](#)). However, the HVS phenomenon is not restricted to MS stars, but is also observed among evolved low-mass stars such as hot subdwarf stars (e.g. [Hirsch et al. 2005](#); [Geier et al. 2015](#); [Németh et al. 2016](#); [Ziegerer et al. 2017](#)) and white dwarfs ([Vennes et al. 2017](#); [Shen et al. 2018](#); [Raddi et al. 2019](#)). Interestingly, kinematic studies excluded the Hills scenario for those early-type stars, suggesting that they are the surviving remnants of double-detonation supernova Ia explosions ([Geier et al. 2015](#); [Vennes et al. 2017](#)). Several claims for unbound late-type stars have been rejected ([Ziegerer et al. 2015](#); [Boubert et al. 2018](#)), which is why early-type stars constitute the main component of the known HVS population. In addition to the late B-type stars from the HVS survey of [Brown et al. \(2014\)](#), even more massive and younger MS stars have been suggested in the pre-*Gaia* era to potentially escape from our Galaxy ([Edelmann et al. 2005](#); [Heber et al. 2008](#); [Irrgang et al. 2010](#); [Zheng et al. 2014](#); [Huang et al. 2017](#); [Li et al. 2018](#)), albeit with a proposed origin in the Galactic disk rather than in the Galactic center for some of them, thus ruling out the Hills mechanism. These high-velocity MS stars were thought to be extreme cases of the well-known class of disk runaway stars.

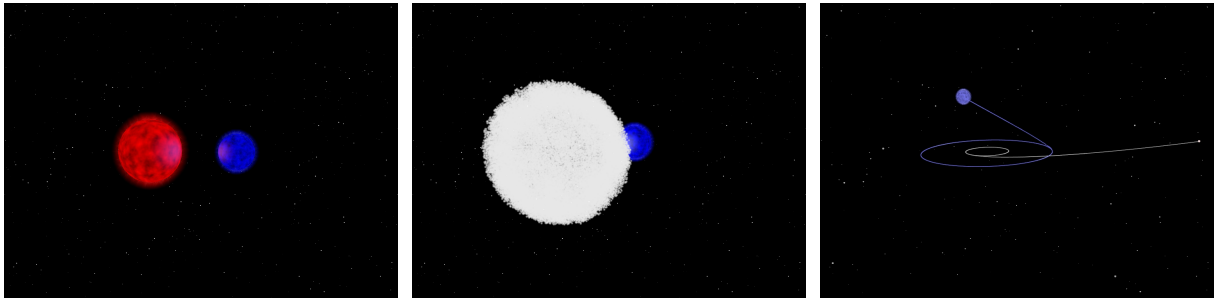


Figure 12. Snapshots illustrating the disruption of a binary system by a supernova explosion. The primary component (red) of an initially bound system (*left*) undergoes a core-collapse supernova explosion (*middle*), which renders the secondary star (blue) and the supernova remnant (white) unbound (*right*). An animated version of this figure is available [online](#).

4.2 Runaway stars

Two “classical” mechanisms have been suggested decades ago for the ejection of runaway stars.

4.2.1 Binary supernova scenario

[Blaauw \(1961\)](#) proposed a binary supernova scenario, where the secondary star of a close binary system is ejected when the binary system is disrupted by the core-collapse explosion of the more massive primary, see Fig. 12. Population synthesis models indicate that only for a small fraction, that is, less than 1%, ejection velocities above 200 km s^{-1} ([Portegies Zwart 2000](#)) or even above 60 km s^{-1} ([Renzo et al. 2019](#)) can be reached. Only in extremely rare cases when a very compact system is torn apart, higher velocities can be achieved. [Tauris \(2015\)](#) studied the ejection of stars of 3.5 and $10 M_{\odot}$, respectively, and found upper limits for the supernova ejection scenario of 540 and 320 km s^{-1} in the most favorable conditions. Such stars could reach their local Galactic escape velocity if the ejection happens to occur in the direction of Galactic rotation.

4.2.2 Dynamical ejection scenario

The second mechanism to create runaway stars is dynamical ejection via three- or four-body interactions (see Fig. 13) in a dense stellar environment ([Poveda et al. 1967](#)). N-body simulations of the dynamical ejection of massive stars from moderately massive star clusters by [Oh & Kroupa \(2016\)](#) show that only very few stars with masses lower than $5 M_{\odot}$ are ejected from a young star cluster with $3000 M_{\odot}$ at more than 100 km s^{-1} . [Perets & Šubr \(2012\)](#) carried out similar N-body simulations for star cluster dynamics and concluded that runaways with velocities $> 300 \text{ km s}^{-1}$ are ejected at rates that are too low to explain a significant fraction of the observed candidate HVSs in the Galactic halo.

4.2.3 Dynamical ejection and subsequent supernova disruption

A combination of both mechanisms is also conceivable. A massive, tightly bound binary may be ejected from a dense, massive stellar cluster, and thereafter, the primary explodes as a core-collapse supernova. Numerical experiments by [Perets & Šubr \(2012\)](#) indicate that no binaries

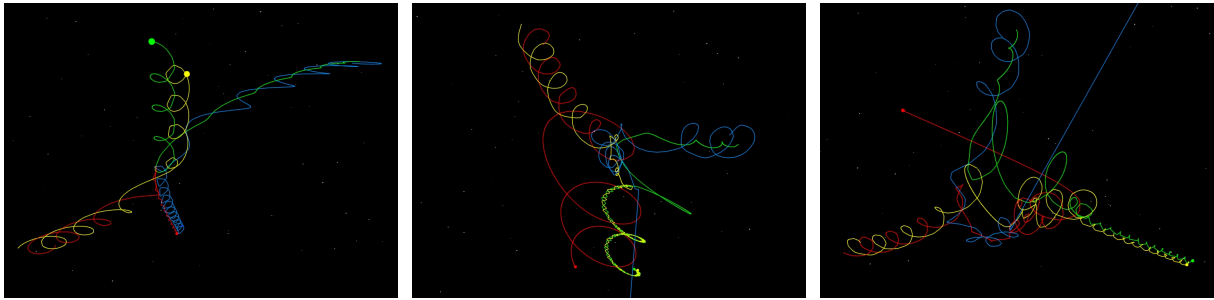


Figure 13. Dynamical binary-binary interactions visualized with the help of trajectories. Two initially separated binary systems – red/yellow and blue/green – interact via a spatially close encounter resulting in an exchange of partners (*left*), formation of a hierarchical triplet system and ejection of the blue star (*middle*), or formation of a new binary system and ejection of the blue and red stars (*right*). Animated versions of these figures are available online: [left](#), [middle](#), [right](#).

are ejected by dynamical ejections with velocities in excess of 150 km s^{-1} . Hence, the combined scenario would shift the speed limit of the binary supernova scenario by such an amount in the most favorable, though very unlikely, case of a perfect alignment between ejection vectors.

4.3 High-velocity early-type stars in the *Gaia* era based on DR2

4.3.1 Revisiting the most promising HVS candidates from the HVS survey

In preparation for the second data release (DR2) of *Gaia*, we reanalyzed the spectra of the 14 most promising HVS candidates from the HVS survey (Brown et al. 2014) – using our improved analysis strategy presented in Sect. 2 – in order to refine their stellar ages and spectrophotometric distances (see Irrgang et al. 2018b, appended). The latter are key ingredients for kinematic studies of HVSs because these objects are usually so far away that *Gaia* parallaxes are still too uncertain to draw firm conclusions. The subsequent kinematic investigation of those 14 objects based on *Gaia* DR2 proper motions provided first indications for the idea that a large portion of the known HVS candidates do not originate in the Galactic center and hence via the Hills mechanism but are actually runaway stars from the Galactic disk, with some of them having ejection velocities in excess of what is possible in the framework of the two classical runaway scenarios mentioned in Sect. 4.2 (see Irrgang et al. 2018a, appended).

4.3.2 An extreme runaway B star challenging classical ejection mechanisms

This idea was further corroborated by our discovery of a new extreme disk runaway star, PG 1610+062, which is an SPB star bright enough to be studied in detail. Our kinematic analysis revealed that this object was probably ejected from the Carina-Sagittarius spiral arm at a velocity of $550 \pm 40 \text{ km s}^{-1}$ (see Fig. 14), granting it place in the top five of the most extreme disk runaway MS stars known at that time (see Irrgang et al. 2019, appended).

4.3.3 Revisiting (almost) all HVS candidates from the HVS survey

A later study covering 40 of the 42 HVS candidates from the HVS survey lead to similar conclusions, namely, that the Galactic center is disqualified as a possible place of origin for almost all

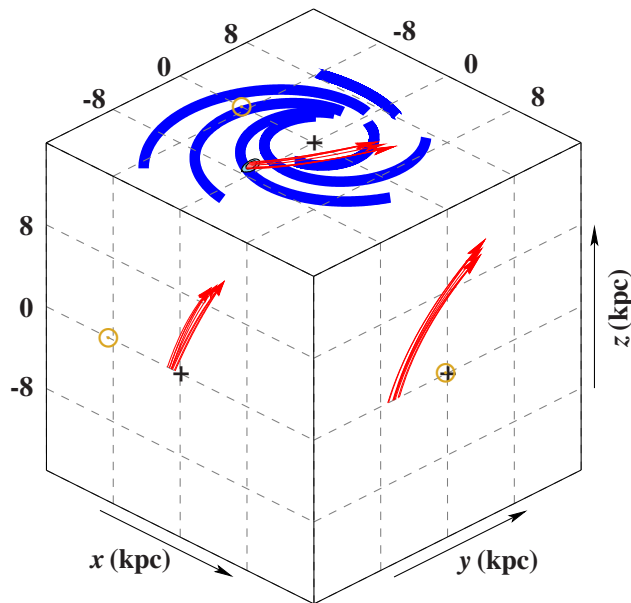


Figure 14. Three-dimensional trajectory of PG 1610+062 in a Galactic Cartesian coordinate system in which the z -axis points to the Galactic north pole. The nine trajectories (red lines; arrows indicate the star’s current position) are computed in Galactic mass model I of [Irrgang et al. \(2013\)](#) and illustrate the effects of uncertainties in the distance, proper motions, and radial velocity. Orbits were computed back in time until they reached the Galactic plane. The thick blue solid lines schematically represent the loci of the spiral arms at the time of plane crossing. The current positions of the Sun and the Galactic center are marked by a yellow circled dot (\odot) and a black plus sign ($+$), respectively. From [Irrgang et al. \(2019\)](#).

of the 18 targets that had a more or less well-constrained spatial origin. Moreover, our spectral reanalysis provided atmospheric parameters and thus spectrophotometric distances of significantly improved precision and accuracy, naturally solving the issue that some objects were lying below the zero-age MS (see Fig. 15), a result that was barely compatible with a MS HVS nature (see [Kreuzer et al. 2020](#), appended).

4.3.4 Searching for new runaway blue MS stars at high Galactic latitudes

In addition to reviewing known high-velocity early-type stars, we also performed a case study to test the capability of *Gaia* at identifying new such stars. To this end, we obtained and examined low-resolution optical spectra of 48 blue stars at high Galactic latitudes with relatively precise parallax measurements and *Gaia* colors that are consistent with those of MS stars with masses above $2 M_{\odot}$. The comparison between distances inferred from spectrophotometry and parallax enabled us to disentangle MS candidates from older BHB candidates, allowing us to identify 12 new MS disk runaway candidates, three of them having ejection velocities that would challenge the classical scenarios if their MS status can be confirmed by follow-up high-resolution spectroscopy (see [Raddi et al. 2021](#), appended).

4.4 High-velocity stars in the *Gaia* era based on EDR3

Finally, we made use of the higher precision of *Gaia* early data release 3 (EDR3; see Fig. 16) to redo the kinematic investigation of 30 of the most extreme MS runaway stars known to date in order to deduce their spatial origins in and their ejection velocities from the Galactic disk. Only three stars in that sample turned out to have past trajectories that are consistent with an origin in the Galactic center (see Fig. 17), most notably S5-HVS 1 ([Koposov et al. 2020](#)), the ejection velocity of which is $1810 \pm 60 \text{ km s}^{-1}$, thus making it the smoking gun for the Hills mechanism and the most extreme MS runaway star known so far. All other program stars were shown to be disk runaways with ejection velocities that sharply contrast at least with the two

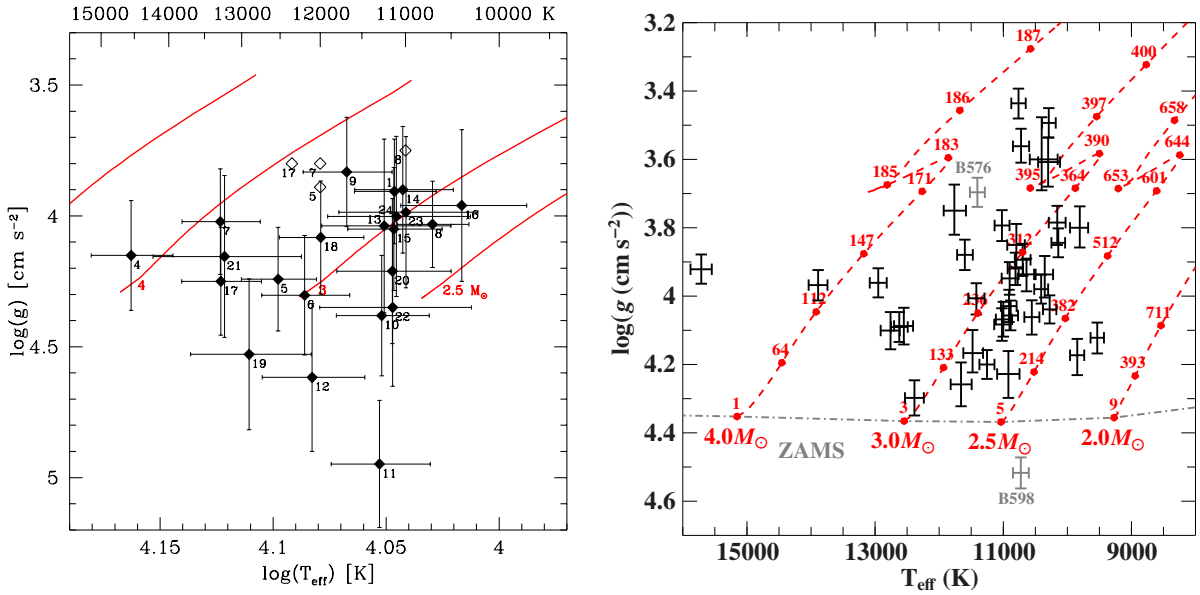


Figure 15. Position of the HVS candidates in the Kiel diagram. *Left panel:* Original atmospheric parameters are compared with Padova solar metallicity MS tracks (red). Several stars lie below or close to the zero-age MS, which is at odds with their claimed MS HVS nature. From [Brown et al. \(2014\)](#). *Right panel:* Our revised atmospheric parameters – which are based on the same spectra but on our improved analysis methodology – are compared with Geneva evolutionary tracks (red). A MS HVS nature is unlikely only for the two objects marked in gray. From [Kreuzer et al. \(2020\)](#). Error bars are 1σ confidence intervals in both panels.

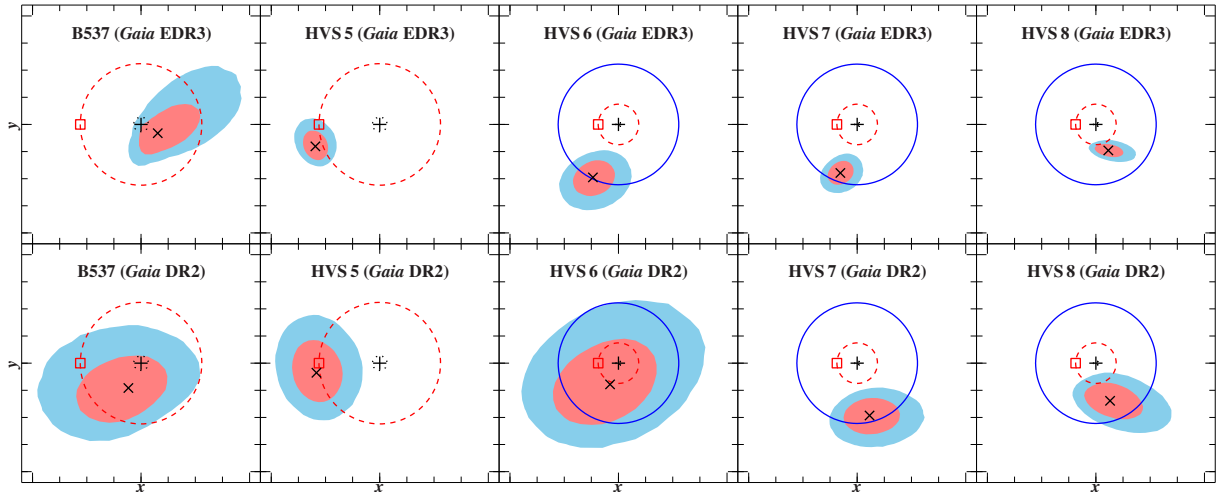


Figure 16. Comparison of the inferred spatial origin within the Galactic plane for five selected HVS candidates based on proper motions from *Gaia* EDR3 (*upper row*) and DR2 (*lower row*) demonstrating the improved precision of EDR3. The most likely plane-crossing point is marked by a black cross, while the shaded areas visualize the corresponding 1σ (light red) and 2σ (light blue) contours. Circles centered at the Galactic center (black plus sign) with radii of 1 kpc (dotted black line), 8.3 kpc (solar circle; dashed red line), and 25 kpc (solid blue line) are shown for reference. The galactocentric coordinate system is Cartesian and right-handed, with the Sun (red square) on the negative x -axis and the z -axis pointing to the Galactic north pole. From [Irrgang et al. \(2021a\)](#).

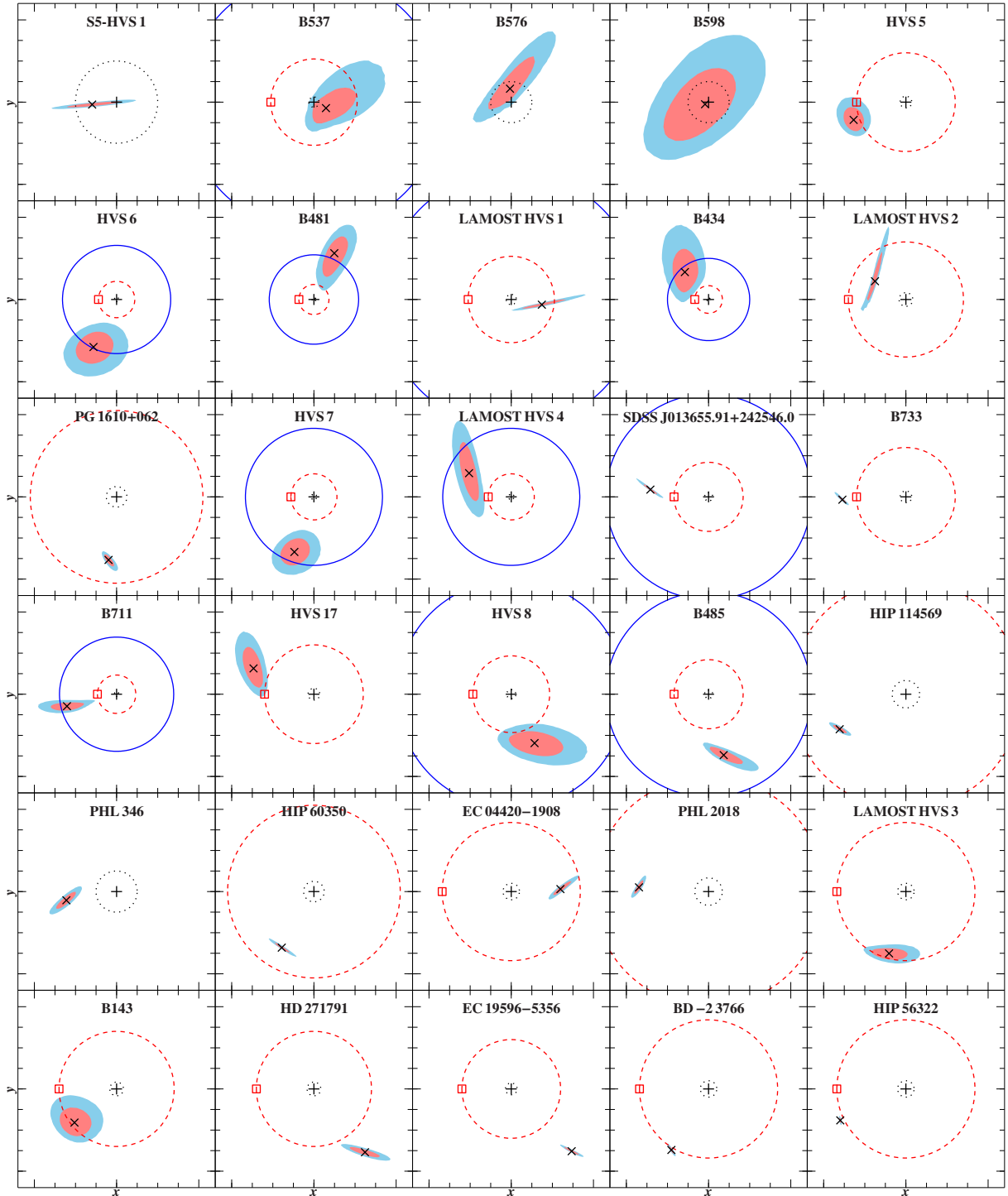


Figure 17. Inferred spatial origin within the Galactic plane for 30 extreme disk runaway stars based on proper motions from *Gaia* EDR3. The objects are arranged with decreasing ejection velocity starting from the top left panel. The most likely plane-crossing point is marked by a black cross, and the shaded areas visualize the corresponding 1σ (light red) and 2σ (light blue) contours. Note the different scales: Circles centered at the Galactic center (black plus sign) with radii of 1 kpc (dotted black line), 8.3 kpc (solar circle; dashed red line), and 25 kpc (solid blue line) are shown for reference, when appropriate. The current position of the Sun (red square) is also marked. From [Irrgang et al. \(2021a\)](#).

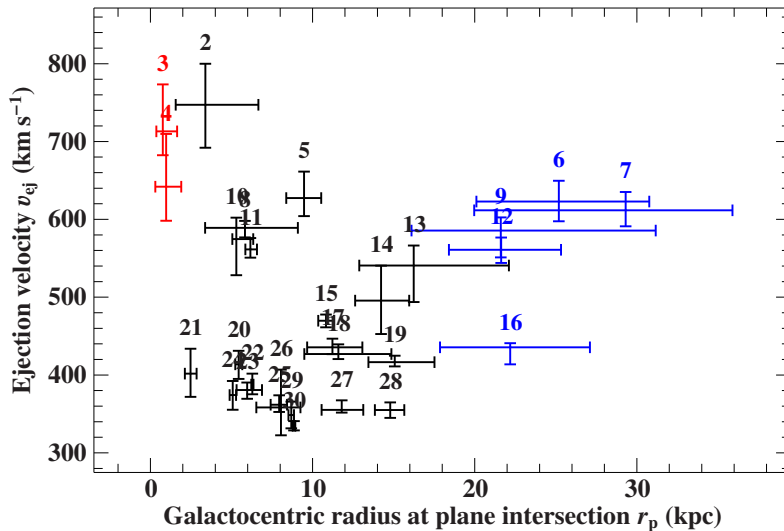


Figure 18. Ejection velocity (relative to the rotating Galactic disk) vs. Galactocentric radius at plane intersection for all 30 program stars except S5-HVS 1, which is beyond the ordinate scale. Error bars are 1σ confidence intervals. The colors mark objects that could stem from the Galactic center (red) or from the outer disk (blue). From [Irrgang et al. \(2021a\)](#).

classical ejection scenarios. While most stars originate from within a Galactocentric radius of 15 kpc, which corresponds to the observed extent of the spiral arms, a group of five stars stems from radii of about 21–29 kpc, see Fig. 18. This indicates a possible link to outer Galactic rings and a potential origin from infalling satellite galaxies (see [Irrgang et al. 2021a](#), appended).

4.5 The need for an alternative ejection mechanism

Driven by the *Gaia* space mission, our studies disproved the widely believed assumption that all HVSs originate in the Galactic center via the Hills mechanism. In fact, we demonstrated that almost all of the most extreme high-velocity early-type MS stars are actually runaway stars from the Galactic disk. Moreover, we argued that the ejection velocities of these extreme disk-runaway stars exceed the predicted limits of the classical scenarios for the production of runaway stars, which then hints at the existence of an as yet unknown or neglected but powerful disk-ejection mechanism. Close encounters with very massive stars or intermediate-mass black holes offer, in principle, a straightforward explanation (see, e.g., [Irrgang et al. 2018a](#) and references therein). The latter option is particularly interesting because no intermediate-mass black hole is currently known in the Galactic disk. However, the rates at which those strong dynamical interactions may occur are not well constrained because the actual number of massive perturbers and the conditions in their host clusters are uncertain (see, e.g., [Hattori et al. 2019](#)). Our observational findings can help to guide theory in this respect, which may eventually lead to a better understanding of (massive) star formation and their evolution in dense stellar environments.

References

- Aerts, C., Christensen-Dalsgaard, J., & Kurtz, D. W. 2010, *Asteroseismology* (London: Springer)
- Arny, T. 1990, *Vistas in Astronomy*, 33, 211
- Bahcall, J. N. 2000, *JRASC*, 94, 219
- Baran, A. S., Østensen, R. H., Heber, U., **Irrgang, A.**, et al. 2021, *MNRAS*, 503, 2157
- Beauchamp, A., Wesemael, F., & Bergeron, P. 1997, *ApJS*, 108, 559
- Belczynski, K., Hirschi, R., Kaiser, E. A., et al. 2020, *ApJ*, 890, 113
- Blaauw, A. 1961, *Bull. Astron. Inst. Neth.*, 15, 265
- Boubert, D., Guillochon, J., Hawkins, K., et al. 2018, *MNRAS*, 479, 2789
- Brott, I., de Mink, S. E., Cantiello, M., et al. 2011, *A&A*, 530, A115
- Brown, W. R. 2015, *ARA&A*, 53, 15
- Brown, W. R., Geller, M. J., & Kenyon, S. J. 2014, *ApJ*, 787, 89
- Brown, W. R., Geller, M. J., Kenyon, S. J., & Kurtz, M. J. I. 2005, *ApJ*, 622, L33
- Calcaferro, L. M., Althaus, L. G., & Córscico, A. H. 2018, *A&A*, 614, A49
- Dorsch, M., Latour, M., Heber, U., **Irrgang, A.**, et al. 2020, *A&A*, 643, A22
- Driebe, T., Schoenberner, D., Bloeker, T., & Herwig, F. 1998, *A&A*, 339, 123
- Edelmann, H., Napiwotzki, R., Heber, U., Christlieb, N., & Reimers, D. 2005, *ApJ*, 634, L181
- Ekström, S., Georgy, C., Eggenberger, P., et al. 2012, *A&A*, 537, A146
- Eldridge, J. J., Stanway, E. R., Breivik, K., et al. 2020, *MNRAS*, 495, 2786
- Fitzpatrick, E. L., Massa, D., Gordon, K. D., Bohlin, R., & Clayton, G. C. 2019, *ApJ*, 886, 108
- Gaia Collaboration, Prusti, T., de Bruijne, J. H. J., et al. 2016, *A&A*, 595, A1
- Geier, S., Fürst, F., Ziegerer, E., Kupfer, T., Heber, U., **Irrgang, A.**, et al. 2015, *Science*, 347, 1126
- Giddings, J. R. 1981, PhD thesis, Univ. London
- Gigosos, M. A. & González, M. Á. 2009, *A&A*, 503, 293
- Götberg, Y., de Mink, S. E., Groh, J. H., et al. 2018, *A&A*, 615, A78
- Groh, J. H., Farrell, E. J., Meynet, G., et al. 2020, *ApJ*, 900, 98
- Handler, G., Pigulski, A., Daszyńska-Daszkiewicz, J., **Irrgang, A.**, et al. 2019, *ApJ*, 873, L4
- Hattori, K., Valluri, M., Castro, N., et al. 2019, *ApJ*, 873, 116
- Heber, U., Edelmann, H., Napiwotzki, R., Altmann, M., & Scholz, R. D. 2008, *A&A*, 483, L21
- Heber, U., **Irrgang, A.**, & Schaffenroth, J. 2018, *Open Astronomy*, 27, 35
- Hills, J. G. 1988, *Nature*, 331, 687
- Hirsch, H. A., Heber, U., O'Toole, S. J., & Bresolin, F. 2005, *A&A*, 444, L61
- Huang, Y., Liu, X. W., Zhang, H. W., et al. 2017, *ApJ*, 847, L9
- Hubeny, I., Hummer, D. G., & Lanz, T. 1994, *A&A*, 282, 151
- Hummer, D. G. & Mihalas, D. 1988, *ApJ*, 331, 794
- Irrgang, A.**, Desphande, A., Moehler, S., Mugrauer, M., & Janousch, D. 2016, *A&A*, 591, L6
- Irrgang, A.**, Dimpel, M., Heber, U., & Raddi, R. 2021a, *A&A*, 646, L4
- Irrgang, A.**, Geier, S., Heber, U., et al. 2021b, *A&A*, 650, A102
- Irrgang, A.**, Geier, S., Heber, U., Kupfer, T., & Fürst, F. 2019, *A&A*, 628, L5
- Irrgang, A.**, Geier, S., Kreuzer, S., Pelisoli, I., & Heber, U. 2020b, *A&A*, 633, L5
- Irrgang, A.**, Kreuzer, S., & Heber, U. 2018a, *A&A*, 620, A48
- Irrgang, A.**, Kreuzer, S., Heber, U., & Brown, W. 2018b, *A&A*, 615, L5
- Irrgang, A.**, Przybilla, N., Heber, U., et al. 2014, *A&A*, 565, A63
- Irrgang, A.**, Przybilla, N., Heber, U., Nieva, M. F., & Schuh, S. 2010, *ApJ*, 711, 138
- Irrgang, A.**, Przybilla, N., & Meynet, G. 2022, *Nature Astronomy*, 6, 1414
- Irrgang, A.**, Wilcox, B., Tucker, E., & Schiefelbein, L. 2013, *A&A*, 549, A137
- Kaplan, D. L., Kupfer, T., Nice, D. J., **Irrgang, A.**, et al. 2016, *ApJ*, 826, 86

- Koch, D. G., Borucki, W. J., Basri, G., et al. 2010, *ApJ*, 713, L79
- Koposov, S. E., Boubert, D., Li, T. S., et al. 2020, *MNRAS*, 491, 2465
- Kreuzer, S. 2021, PhD thesis, Friedrich-Alexander-Universität Erlangen-Nürnberg (FAU)
- Kreuzer, S., **Irrgang, A.**, & Heber, U. 2020, *A&A*, 637, A53
- Kupfer, T., Bauer, E. B., Burdge, K. B., . . . , **Irrgang, A.**, et al. 2020, *ApJ*, 898, L25
- Kurucz, R. L. 1996, in *Model Atmospheres and Spectrum Synthesis*, ed. S. J. Adelman, F. Kupka, & W. W. Weiss (San Francisco: ASP), 160
- Lara, N., González, M. Á., & Gigosos, M. A. 2012, *A&A*, 542, A75
- Latour, M., Chayer, P., Green, E. M., **Irrgang, A.**, & Fontaine, G. 2018, *A&A*, 609, A89
- Latour, M., Heber, U., **Irrgang, A.**, et al. 2016, *A&A*, 585, A115
- Lennon, D. J., Maíz Apellániz, J., **Irrgang, A.**, et al. 2021, *A&A*, 649, A167
- Li, Y.-B., Luo, A. L., Zhao, G., et al. 2018, *AJ*, 156, 87
- Liu, J., Zhang, H., Howard, A. W., et al. 2019, *Nature*, 575, 618
- Németh, P., Ziegerer, E., **Irrgang, A.**, et al. 2016, *ApJ*, 821, L13
- Nieva, M. F. & Przybilla, N. 2006, *ApJ*, 639, L39
- Nieva, M. F. & Przybilla, N. 2007, *A&A*, 467, 295
- Nieva, M. F. & Przybilla, N. 2008, *A&A*, 481, 199
- Nieva, M. F. & Przybilla, N. 2012, *A&A*, 539, A143
- Ochsenbein, F., Bauer, P., & Marcout, J. 2000, *A&AS*, 143, 23
- Oh, S. & Kroupa, P. 2016, *A&A*, 590, A107
- Perets, H. B. & Šubr, L. 2012, *ApJ*, 751, 133
- Portegies Zwart, S. F. 2000, *ApJ*, 544, 437
- Poveda, A., Ruiz, J., & Allen, C. 1967, *Bol. Obs. Tonantzintla Tacubaya*, 4, 86
- Przybilla, N., Butler, K., Becker, S. R., & Kudritzki, R. P. 2006, *A&A*, 445, 1099
- Przybilla, N., Nieva, M.-F., & Butler, K. 2011, in *Journal of Physics Conference Series*, Vol. 328, *Journal of Physics Conference Series*, 012015
- Raddi, R., Hollands, M. A., Koester, D., et al. 2019, *MNRAS*, 489, 1489
- Raddi, R., **Irrgang, A.**, Heber, U., Schneider, D., & Kreuzer, S. 2021, *A&A*, 645, A108
- Renzo, M., Zapartas, E., de Mink, S. E., et al. 2019, *A&A*, 624, A66
- Ricker, G. R., Vanderspek, R., Winn, J., et al. 2016, in *Society of Photo-Optical Instrumentation Engineers (SPIE) Conference Series*, Vol. 9904, *Space Telescopes and Instrumentation 2016: Optical, Infrared, and Millimeter Wave*, ed. H. A. MacEwen, G. G. Fazio, M. Lystrup, N. Batalha, N. Siegler, & E. C. Tong, 99042B
- Sahoo, S. K., Baran, A. S., Heber, U., . . . , **Irrgang, A.**, et al. 2020, *MNRAS*, 495, 2844
- Schaffenroth, V., Casewell, S. L., Schneider, D., . . . , **Irrgang, A.**, et al. 2021, *MNRAS*, 501, 3847
- Schindewolf, M., Németh, P., Heber, U., . . . , **Irrgang, A.**, et al. 2018, *A&A*, 620, A36
- Schneider, D., **Irrgang, A.**, Heber, U., Nieva, M. F., & Przybilla, N. 2018, *A&A*, 618, A86
- Shen, K. J., Boubert, D., Gänsicke, B. T., et al. 2018, *ApJ*, 865, 15
- Shenar, T., Bodensteiner, J., Abdul-Masih, M., et al. 2020, *A&A*, 639, L6
- Silvotti, R., Schaffenroth, V., Heber, U., . . . , **Irrgang, A.**, et al. 2021, *MNRAS*, 500, 2461
- Tauris, T. M. 2015, *MNRAS*, 448, L6
- Taylor, M. B. 2006, in *Astronomical Society of the Pacific Conference Series*, Vol. 351, *Astronomical Data Analysis Software and Systems XV*, ed. C. Gabriel, C. Arviset, D. Ponz, & S. Enrique, 666
- Tremblay, P. E. & Bergeron, P. 2009, *ApJ*, 696, 1755
- Vennes, S., Németh, P., Kawka, A., et al. 2017, *Science*, 357, 680
- Zheng, Z., Carlin, J. L., Beers, T. C., et al. 2014, *ApJ*, 785, L23
- Ziegerer, E., Heber, U., Geier, S., **Irrgang, A.**, et al. 2017, *A&A*, 601, A58
- Ziegerer, E., Volkert, M., Heber, U., **Irrgang, A.**, et al. 2015, *A&A*, 576, L14

Acknowledgements

I am very grateful to Stefan Dreizler, Uli Katz, and Uli Heber for mentoring this habilitation project. Moreover, I acknowledge funding

1. by the Erlangen Centre for Astroparticle Physics for spending two months at the Instituto de Astrofísica de Canarias where Sergio Simón-Díaz and Artemio Herrero kindly hosted me,
2. of a Feodor Lynen Research Fellowship for experienced researchers by the Humboldt foundation,
3. of a postdoc position through grant IR190/1-1 by the German Research Foundation (DFG) which helped to obtain part of the results presented in this work.

Finally, special thanks go again to Uli Heber for his great support, encouragement, and advice over the past twelve years.

Appended papers

Modeling of stellar atmospheres and spectrophotometric analyses

Irrgang, A., Kreuzer, S., Heber, U., Brown W.: *A quantitative spectral analysis of 14 hypervelocity stars from the MMT survey*, 2018, [Astronomy & Astrophysics](#), 615, L5

Schneider, D., **Irrgang, A.**, Heber, U., Nieva, M. F., Przybilla, N.: *NLTE spectroscopic analysis of the ^3He anomaly in subluminous B-type stars*, 2018, [Astronomy & Astrophysics](#), 618, A86

Irrgang, A., Geier, S., Heber, U., Kupfer, T., Fürst, F.: *PG 1610+062: a runaway B star challenging classical ejection mechanisms*, 2019, [Astronomy & Astrophysics](#), 628, L5

Lennon, D. J., Maíz Apellániz, J., **Irrgang, A.**, Bohlin, R., Deustua, S., Dufton, P. L., Simón-Díaz, S., Herrero, A., Casares, J., Muñoz-Darias, T., Smartt, S. J., González Hernández, J. I., de Burgos, A.: *Hubble spectroscopy of LB-1: Comparison with B+black-hole and Be+stripped-star models*, 2021, [Astronomy & Astrophysics](#), 649, A167

Constraints on stellar models from pulsating and/or stripped stars

Irrgang, A., Desphande, A., Moehler, S., Mugrauer, M., Janousch, D.: *The slowly pulsating B-star 18 Pegasi: A testbed for upper main sequence stellar evolution*, 2016, [Astronomy & Astrophysics](#), 591, L6

Irrgang, A., Geier, S., Kreuzer, S., Pelisoli, I., Heber, U.: *A stripped helium star in the potential black hole binary LB-1*, 2020, [Astronomy & Astrophysics](#), 633, L5

Irrgang, A., Geier, S., Heber, U., Kupfer, T., El-Badry, K., Bloemen, S.: *A proto-helium white dwarf stripped by a substellar companion via common-envelope ejection. Uncovering the true nature of a candidate hypervelocity B-type star*, 2021, [Astronomy & Astrophysics](#), 650, A102

Irrgang, A., Przybilla, N., Meynet, G.: *γ Columbae as a recently stripped pulsating core of a massive star*, 2022, [Nature Astronomy](#), 6, 1414

Origin of runaway and hypervelocity stars

Irrgang, A., Kreuzer, S., Heber, U.: *Hypervelocity stars in the Gaia era. Runaway B stars beyond the velocity limit of classical ejection mechanisms*, 2018, [Astronomy & Astrophysics](#), 620, A48

Kreuzer, S., **Irrgang, A.**, Heber, U.: *Hypervelocity stars in the Gaia era. Revisiting the most extreme stars from the MMT HVS survey*, 2020, [Astronomy & Astrophysics](#), 637, A53

Raddi, R., **Irrgang, A.**, Heber, U., Schneider, D., Kreuzer, S.: *Runaway blue main-sequence stars at high Galactic latitudes. Target selection with Gaia and spectroscopic identification*, 2021, [Astronomy & Astrophysics](#), 645, A108

Irrgang, A., Dimpel, M., Heber, U., Raddi, R.: *Blue extreme disk-runaway stars with Gaia EDR3*, 2021, [Astronomy & Astrophysics](#), 646, L4